5-2018

The Effect of Heat Generation in the Railroad Bearing Thermoplastic Elastomer Suspension Element on the Thermal Behavior of Railroad Bearing Assembly

Oscar Osvaldo Rodriguez
The University of Texas Rio Grande Valley

THE EFFECT OF HEAT GENERATION IN THE RAILROAD BEARING THERMOPLASTIC ELASTOMER SUSPENSION ELEMENT ON THE THERMAL BEHAVIOR OF RAILROAD BEARING ASSEMBLY

A Thesis

by

OSCAR OSVALDO RODRIGUEZ

Submitted to the Graduate College of
The University of Texas Rio Grande Valley
In partial fulfillment of the requirements for the degree of

MASTER OF SCIENCE ENGINEERING

May 2018

Major Subject: Mechanical Engineering

THE EFFECT OF HEAT GENERATION IN THE RAILROAD BEARING THERMOPLASTIC ELASTOMER SUSPENSION ELEMENT ON THE THERMAL BEHAVIOR OF RAILROAD BEARING ASSEMBLY

A Thesis
by
OSCAR OSVALDO RODRIGUEZ

COMMITTEE MEMBERS

Dr. Constantine Tarawneh
Chair of Committee

Dr. Arturo Fuentes
Co-Chair of Committee

Dr. Robert Jones
Committee Member

May 2018

ABSTRACT

Rodriguez, Oscar O., The Effect of Heat Generation in the Railroad Bearing Thermoplastic Elastomer Suspension Element on the Thermal Behavior of Railroad Bearing Assembly. Master of Science Engineering (MSE), May, 2018, 64 pp., 12 tables, 40 figures, 11 references.

Understanding the internal heat generation of the railroad bearing elastomer suspension element during operation is essential to predict its dynamic response and structural integrity, as well as to predict the thermal behavior of the complete railroad bearing assembly including the bearing adapter. The latter is essential for sensor selection and placement within the adapter (e.g., typical temperature sensors have operating ranges of up to 125°C or 257°F). The internal heat generation is a function of the loss modulus, strain, and frequency. Based on experimental studies, estimations of internally generated heat within the thermoplastic elastomer pad were obtained. The calculations show that the pad internal heat generation is impacted by temperature and frequency. However, during service operation, exposure of the suspension pad to loading frequencies above 10 Hz is less likely to occur. Therefore, internal heat generation values that have a significant impact on the suspension pad steady-state temperature are less likely to be reached. An experimentally validated finite element thermal model that can be used to obtain temperature distribution maps of complete bearing assemblies in service operation conditions is presented. This thesis summarizes the work done to investigate the effect of the internal heat generation in the thermoplastic elastomer suspension element on the thermal behavior of the railroad bearing assembly.

DEDICATION

I would like to dedicate this thesis to my family. My parents, Oscar and Maribel, thank you for all the support and motivation you have provided me throughout the years as a student. Thank you for your guidance in life and towards my education. This would have not been possible without your hard work. This incredible achievement is also yours. My siblings, Odalys and Orlando, thank you for being a motivation towards continuing my academic studies, thank you for making me your role model and allowing me to become a great example for both. Daniela, thank you for always being there for me regardless of the circumstances, for always putting a smile on my face and for being my person, you truly are amazing. Thank you all for your unconditional love and patience.

Me gustaría dedicar esta tesis a mi familia. Mis padres, Oscar y Maribel, gracias por todo el apoyo y la motivación que me han brindado a lo largo de los años como estudiante. Gracias por su guía en la vida y en mi educación. Esto no hubiera sido posible sin su arduo trabajo. Este logro increíble también es suyo. Mis hermanos, Odalys y Orlando, gracias por ser una motivación para continuar mis estudios académicos, gracias por hacerme su modelo a seguir y por permitir convertirme en un gran ejemplo para ambos. Daniela, gracias por siempre estar ahí para mí, independientemente de las circunstancias, por siempre poner una sonrisa en mi cara y por ser mi persona, realmente eres increíble. Gracias a todos por su amor y paciencia incondicional.

ACKNOWLEDGMENTS

I would like to begin by thanking Dr. Constantine Tarawneh, without your help, this thesis would not be possible. Thank you for your hard work, commitment, and dedication towards this work and my education. Thank you for being a great leader and always pushing me to become the best version of myself, you have truly prepared me for what is to come. Thank you for giving me the opportunity to be part of the greatest research team in the university.

Dr. Arturo Fuentes, thank you for your infinite input towards this work and my education. Your mentorship and guidance throughout these years allowed me to become a better student and a better person. Thank you for that extra push and the encouragement to always think further. Your insight towards this work is beyond compare, without your help, this thesis would not be possible.

Dr. Robert Jones, thank you for the tremendous amount of help, the extensive advice, and guidance you provided towards this project. Thank you for always pushing me to do more. Your expertise in the materials field applied to this work are greatly appreciated.

Additionally, I would like to thank James Aranda and Joseph Montalvo for helping me with my research. Thank you both for always being available to answer my questions about any modeling issues I encountered. I would like to thank all past and present UTCRS members who have helped me throughout this journey. To my current team, thank you for your hard work and support. It has been a great privilege to work and learn from every single one of you, for that I will forever be grateful. Thank You!

Finally, I would like to acknowledge that this study was made possible by funding provided by The University Transportation Center for Railway Safety (UTCRS), through a USDOT Grant No. DTRT 13-G-UTC59.

TABLE OF CONTENTS

LIST OF TABLES

Page

LIST OF FIGURES

Page

CHAPTER I

INTRODUCTION

Reliable health monitoring of railroad bearings is essential to ensure the safe transport of commodities and goods, and to prevent catastrophic failures in the railroad industry. Between 2010 and 2016, there were approximately 106 freight train derailments that were caused by the overheating of a bearing in one or multiple railcars [1]. To identify distressed bearings in service, conventional railroad bearing health monitoring systems rely on the bearing cup (outer ring) temperature as detected by wayside monitoring systems, spaced at specific distances alongside tracks, to warn of impending failure. Railroad bearing temperatures are monitored by wayside devices called hot-box detectors (HBDs), which use infrared sensors to take snapshots of bearing temperatures as they pass over the detectors to identify bearings that are operating at temperatures greater than 94.4ºC (170ºF) above ambient conditions [2]. Currently, most U.S. railroads tend to track the temperature of each bearing and compare it to the average temperature of all bearings on the same side of the train. Hence, bearings that are "trending" above normal can be identified without waiting for a hot-box detector to be triggered [3]. Railroad bearings that are found to be hot are removed from service for later disassembly and inspection. Generally, the overheating of the bearing can be correlated back to one or more of the common modes of bearing failure such as water or dirt contamination, spalling, broken internal components, damaged seals, improper lubrication, etc. However, in many cases, the hot bearings that are set

out do not exhibit signs of any of the common causes (i.e. non-verified bearings). Researchers continue to place strong emphasis on issues such as the warm trending phenomenon that leads to the unnecessary and costly removal of non-verified bearings. These temperature health monitoring systems, such as the wayside hot-box detectors (HBDs), have helped to reduce the number of freight train derailments significantly since their implementation. However, their limited accuracy prevents them from being a true continuous health monitoring system. New technologies are focusing on a more frequent (i.e. continuous) method to track temperatures of railroad bearings. Since placing sensors directly on the bearing is not practical due to cup indexing during service, the next logical location for such sensors is the bearing adapter, which frequently interfaces with the thermoplastic elastomer suspension pad [4].

1.1 AdapterPlus™ and Thermoplastic Elastomer Suspension Pad

Thermoplastic elastomers (TPE's) are increasingly being used in rail service for load damping and other applications. Like traditional elastomers, they offer benefits including reduction in noise emissions and improved wear and abrasion resistance in metal components that are in contact with such parts, specifically in the bogie (also known as railcar). They are superior to traditional elastomers primarily in their ease of fabrication. The railroad bearing AdapterPlus™, which has replaced many conventional all metal bearing adapters, utilizes the thermoplastic elastomer suspension pad, as shown in Figure 1.1.

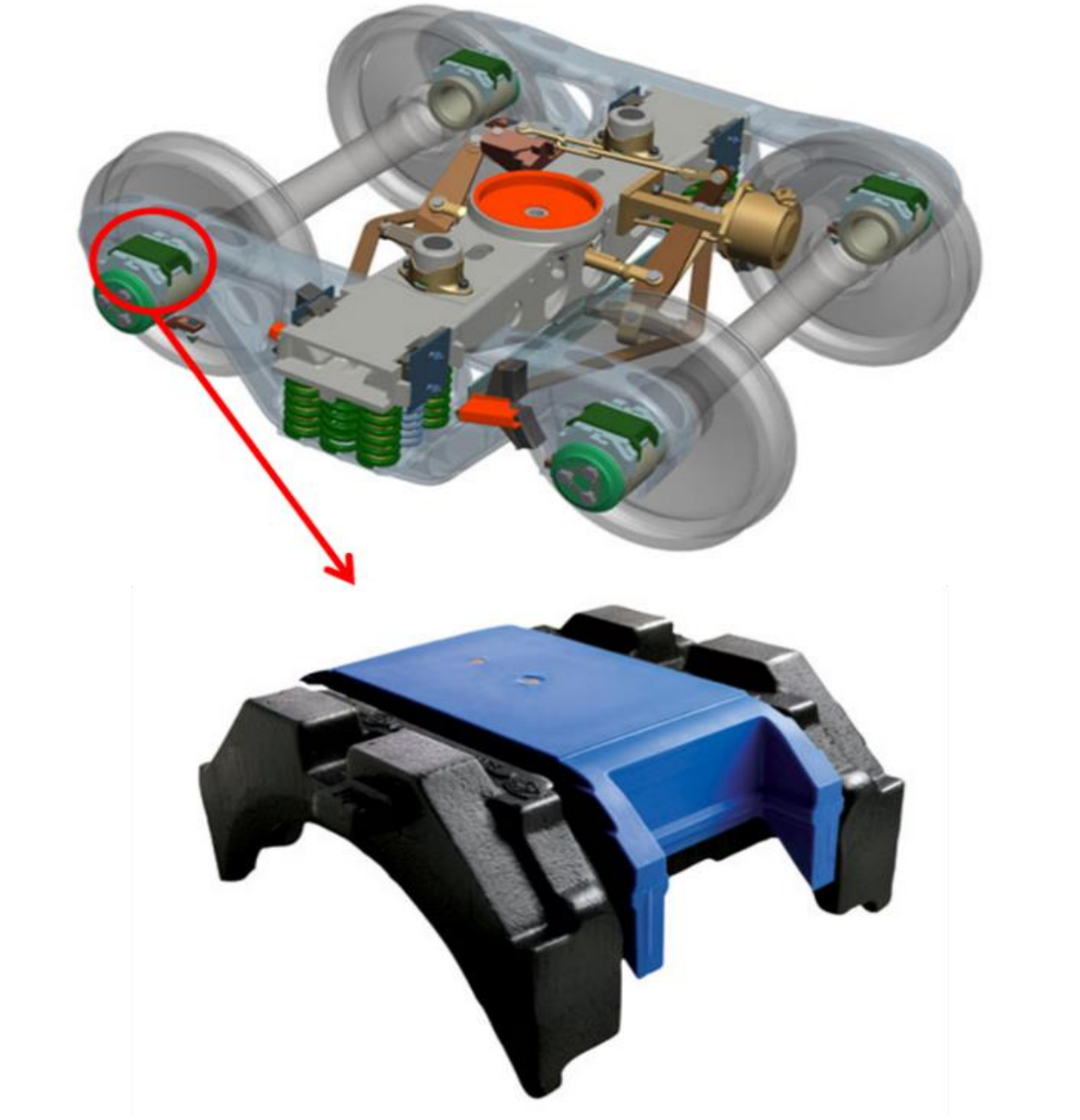

Figure 1.1. Configuration and location of AdapterPlus™ with thermoplastic elastomer steering pad (Blue) within wheel-axle-bearing assembly of the freight car suspension system [5].

The elastomer steering pad, which is implemented in the wheel-axle-bearing assembly of a freight car, as seen in Figure 1.1 , has proved to be extremely beneficial. The purpose of the elastomer pad is to prevent metal-to-metal contact between the bearing adapter and the side frame of the truck. The main benefits of implementing the elastomer steering pad on top of the

bearing adapter include: improvement of axle-to-rail alignment which allows a controlled motion of the wheelset with reduced lateral force in curves, a wheelset life increase of 25%, and an 8% decrease in fuel consumption, among other benefits [5]. However, the suspension element also acts as a partial insulator of heat from the bearing and adapter to the components in contact above the pad.

Moreover, viscoelastic materials, such as the railroad bearing thermoplastic elastomer suspension element (or elastomeric pad), are known to develop self-heating (hysteresis) under cyclic loading, which can lead to undesirable consequences [6]. In general, for viscoelastic materials subjected to a varying load, part of the deformation energy is stored and part is dissipated through internal molecular mechanisms as heat [7], [8]. This hysteresis heating in thermoplastic elastomer materials becomes particularly significant during cyclic loading and is a potential problem, specially, when there is limited opportunity for heat dissipation. The hysteretic dissipation of polymers increases with frequency so a thermal runaway is more likely to be present at higher loading frequencies. When the heat that is produced does not dissipate out of the system, the temperature of the material increases and may potentially impact the structural integrity of the thermoplastic elastomer suspension element and/or the thermal management of the railroad bearing assembly. That is, if no thermal runway is present for the heat to dissipate out of the suspension pad, and the pad is being subjected to high frequency loadings, the internally generated heat is significant and can cause the suspension pad to reach temperatures higher than those of any other component in the bearing assembly. Consequently, as the temperature increases, there is usually a significant decrease in the strength and stiffness of the material, otherwise known as softening. This may lead to the deterioration and degradation of the suspension pad and result in mechanical failure. The behavior of viscoelastic materials during

cyclic load induced failure depends on the material system, stress state, and thermal environment.

1.2 Continuous Research

The work conducted in this study focuses on the effect of the internal heat generation in the railroad thermoplastic elastomer suspension element on the thermal behavior of the railroad bearing assembly. Understanding the impact of the hysteresis heating of the railroad bearing elastomer suspension element during operation is essential to predict its dynamic response and structural integrity, as well as, to predict the thermal behavior of the railroad bearing assembly. For example, since the thermoplastic elastomer suspension element is known to develop hysteresis heating , understanding the thermal behavior of the bearing adapter in combination with the elastomeric pad during operation is essential for sensor selection and placement within the adapter (e.g., typical temperature sensors have operating ranges of up to 125°C or 257°F) [4]. Load and temperature sensors that were developed by the UTCRS research group are currently place right below the suspension element machined into the bearing adapter. The main purpose of these sensors is to continuously monitor the load applied to the railroad bearing and the temperatures of both the adapter and the railroad bearing assembly. If the internally generated heat of the thermoplastic elastomer suspension element is significant, an increase in the temperature of the pad is more likely to occur. As a result, this may affect the readings and can jeopardize the operation of such sensors placed on the adapter.

The work is organized as follows: Chapter 2 presents the experimental studies conducted in order to determine the heat generation due to the hysteresis heating of the thermoplastic elastomer suspension element and the estimated heat generation values obtained. Chapter 3 presents the laboratory experimental setups of the dynamic railroad bearing test rigs and the

operation conditions. Chapter 4 presents the finite element analysis (FEA) conducted in order to obtain temperature maps of the thermoplastic elastomer suspension element and of the railroad bearing assembly and adapter. Finally, Chapter 5 presents a summary of the main conclusions from this work.

CHAPTER II

HEAT GENERATION DUE TO HYSTERESIS HEATING

Understanding the impact of the heat generation due to the hysteresis heating of the railroad bearing elastomer suspension element during operation is essential to predict its dynamic response and structural integrity, as well as, to predict the thermal behavior of the railroad bearing assembly. The following sections focus on the heat generation due to the hysteresis heating that occurs in elastomers used in the compliant suspension element. Experiments consisted of material characterization using a servohydraulic universal material testing system (MTS) and Dynamic Mechanical Analyzer (DMA). The aforementioned experimental characterization of the hysteresis heating was necessary for heat transfer calculations and simulations presented in the Chapter 4.

2.1 MTS Hysteresis Testing

Preliminary findings on the hysteresis heating of the suspension pad were determined by conducting experiments on different 6.3 cm (2.5 in) diameter cylindrical samples of virgin pad material and modified pad material with 5-15% Carbon Nano-Fiber (CNF), as seen in Figure 2.1, to determine the total conductivity of the virgin and modified pad material. The findings show that the 6.3 cm (2.5 in) diameter cylindrical sample of virgin pad material produced temperature increases as high as 25°C (45°F) under loadings ranging between 2.2 kN (500 lb_f) and 24 kN (5500 lb_f) in compression oscillating at a frequency of 10 Hertz at room temperature.

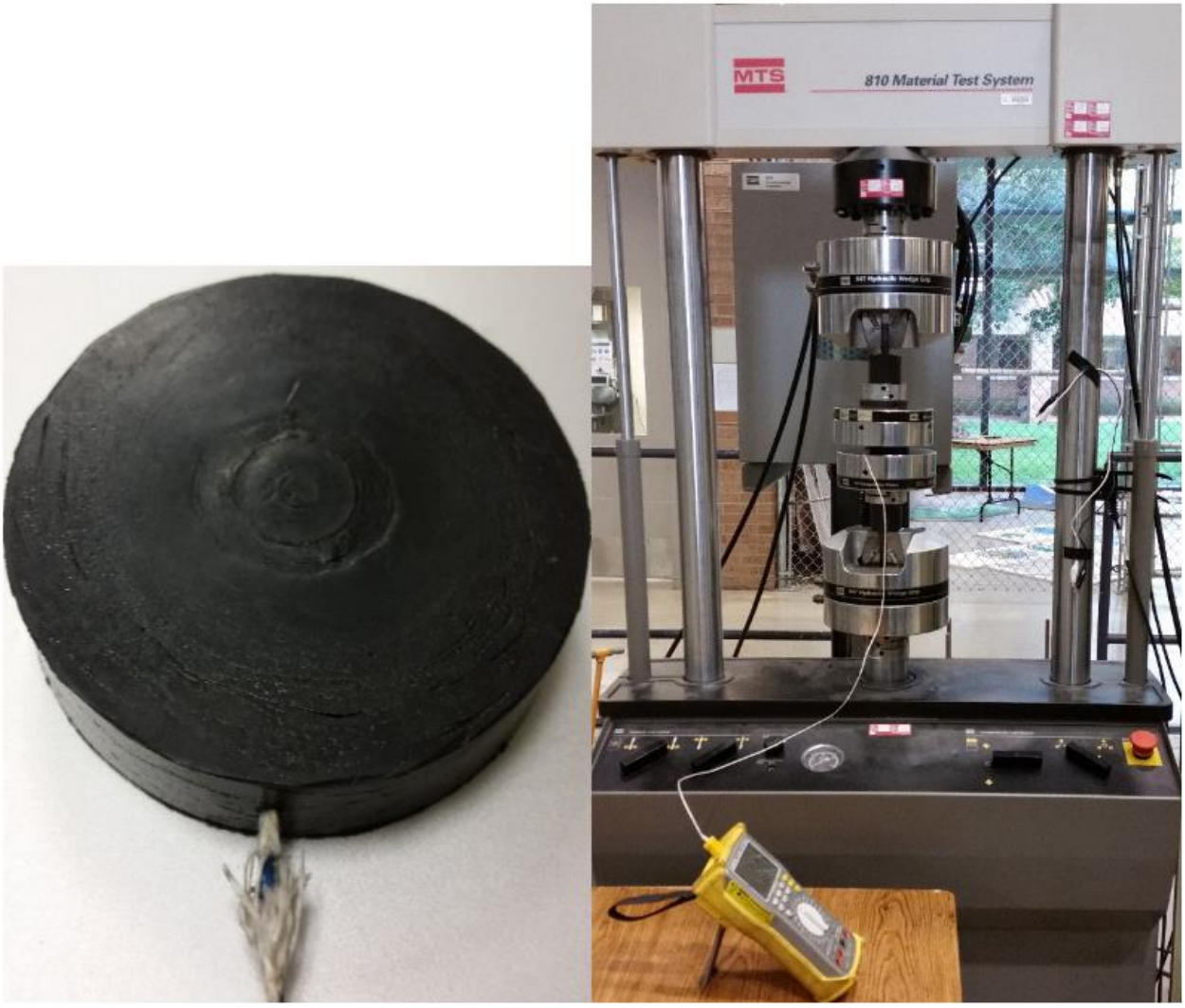

Figure 2.1. Hysteresis heating cylindrical sample of virgin pad material with thermocouple inserted in the specified location (left) and Hysteresis heating test setup on 810 Material Test System (MTS) (right).

Hysteresis tests were conducted on an 810 Material Testing System (MTS) with the setup pictured in Figure 2.1 The setup consisted of a cylindrical sample mounted in-between two MTS 643 compression platens with a K-class thermocouple inserted fully to contact the center-middle area of the sample. The thermocouple is connected to an OMEGA® True RMS SUPERMETER®, which displays the temperature of the thermocouple measurement in degrees Celsius. The tests consisted of rapid repeated cycles of compression under loadings ranging between 2.2 kN (500

lb_f) and 24 kN (5500 lb_f) oscillating at frequencies of 2, 4, 10, 20, 30, and 50 Hertz at room temperature (20ºC or 68ºF).

2.1.1 Low Frequency Hysteresis Tests

The first set of tests were conducted at loading frequencies of 2, 4, 10, and 20 Hz. The initial temperature was documented at time zero before the test sample was loaded. Once loaded, temperature measurements were taken every 30 seconds for the first 5 minutes, followed by every minute for the next 5-10 minutes. A total of 10 minutes of data was collected for 2 and 4 Hz, and 15 minutes of data for 10 and 20 Hz. Multiple tests were run approximately 20 minutes apart for the same oscillating frequency to check for errors and ensure reliability and repeatability.

For loading frequencies of 2, 4, and 10 Hz, the resulting test data sets were neglected due to minimal temperature change (~1-3ºC) of the sample, indicating that regardless of the load magnitude, at frequencies below 10 Hz, the change in the sample's temperature is not significant for short periods of time (i.e. 10-15 minutes). For the loading frequency of 20 Hz, multiple tests were run and the results were fairly similar, having a temperature increase of 5-6ºC (9-10.8ºF). Figure 2.2 displays the comparison curves of the temperature change for the 20 Hz experiments. Both runs for the sample loaded at 20 Hz show the same trend with approximately a 2ºC (3.6ºF) difference at every timed measurement. The difference seen in the equilibrium temperature is due to a combination of variation in the ambient temperature and the temperature of the contacting surfaces of the test fixtures as well as apparent changes in puck microstructure during cycling which increase the hysteretic effect on subsequent cycles.

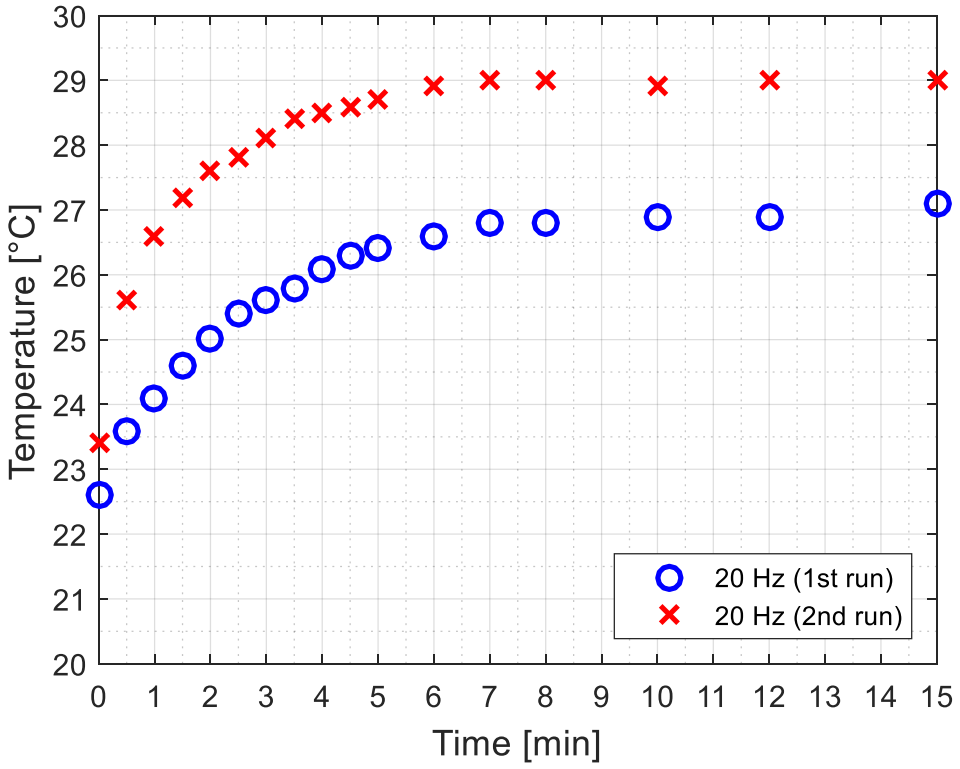

Figure 2.2. Temperature change of cylindrical sample loaded at 20 Hz.

2.1.2 High Frequency Hysteresis Tests

The second set of tests were conducted at loading frequencies of 30 and 50 Hz. The initial temperature was documented at time zero before the test sample was loaded. Once loaded, temperature measurements were taken every 15 seconds for the first 2 minutes, followed by every 30 seconds for the next 3 minutes, and finally every minute for the last 10-15 minutes of testing. A total of 15 minutes of data was acquired for 30 Hz, and 20 minutes of data was collected for 50 Hz. Multiple tests were run approximately 20 minutes apart for the same oscillating frequency to check for errors and ensure reliability and repeatability.

Figure 2.3 displays the comparison curves between the sample temperature change when exposed to loading frequencies of 30 and 50 Hz. When the sample is loaded at higher frequencies, it displays a significant increase in temperature. At 30 Hz, the sample had a temperature increase of 4ºC (7.2ºF), and when loaded at 50 Hz, the sample produced a

temperature increase of 12ºC (21.6ºF). The tests were run again allowing a 20 minute equipment and material cool down in between. This was done in order to check for repeatability and reliability of the results. The second set of experiments all showed a higher increase in temperature compared to the first run of experiments. When the sample was loaded at 30 Hz, it had a temperature increase of 8ºC (14.4ºF), and at 50 Hz, the sample had a temperature increase of 22ºC (39.6ºF). The average of both runs for each frequency are presented in Figure 2.4. The average sample temperature change is used in the model construction.

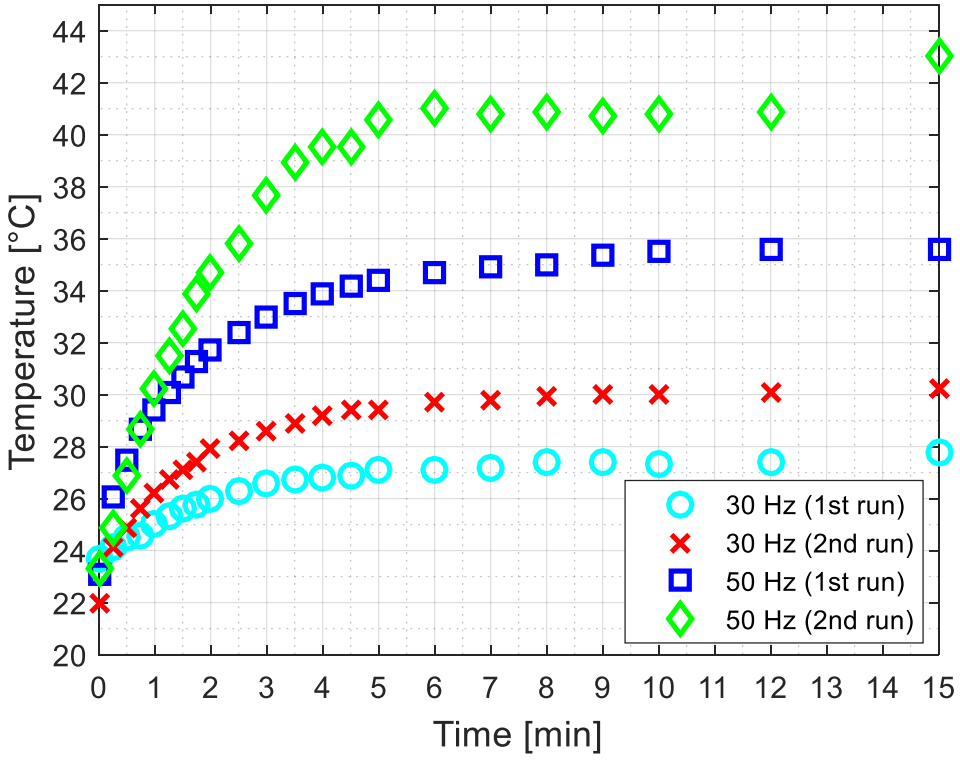

Figure 2.3. Temperature change of cylindrical sample loaded at 30 and 50 Hz (two runs for each loading frequency).

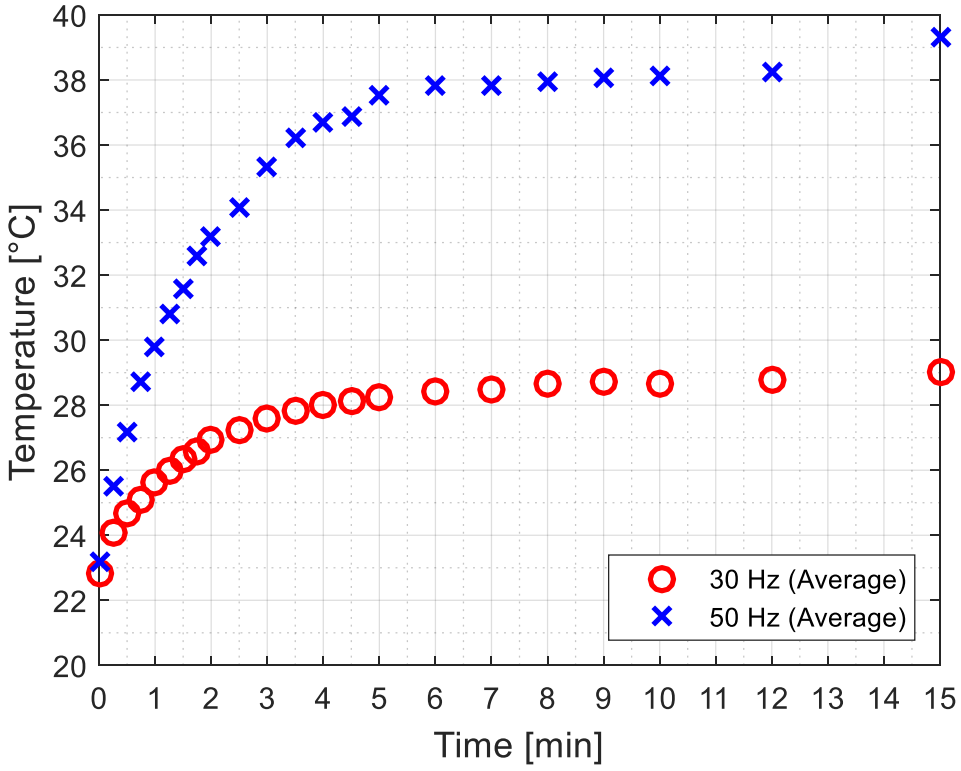

Figure 2.4. Average sample temperature change for both runs of 30 and 50 Hz.

2.2 Dynamic Mechanical Analysis (DMA)

In order to characterize and model the contribution of the elastomer pad to the system energy balance, thermal analysis tests were conducted on samples of virgin pad material. Specifically, the goal was to obtain the mechanical viscoelastic properties (modulus and energy dissipation) of the thermoplastic elastomer suspension pad material. Moreover, in order to measure the mechanical viscoelastic properties of the pad material, dynamic mechanical analysis (DMA) is the proper technique to follow, since DMA is ideal for evaluating time, frequency and temperature dependent material properties. DMA is a technique used to study the viscoelastic behavior of polymers and provides a broad characterization of the elastic (energy storage) and viscous (energy dissipation) behavior of the material over a large range of temperatures and frequencies. The technique subjects a specific sample to a steady-state oscillatory load or displacement while the samples' response is measured. The relatively low thermal mass of the

sample and capabilities of the instrument permit rapid measurement of properties over a wide range of temperatures and frequencies. In a viscoelastic material, the response will have an in-phase and a lagging response. Steady-state oscillation permits separation of these two responses and calculation of the material storage and loss moduli.

Analysis was performed using a TA Instruments Model Q800 Dynamic Mechanical Analyzer (DMA), pictured in Figure 2.5, running the TA Rheology Advantage software. The Q800 DMA measures the viscoelastic properties of a material as it is being deformed under a controlled stress or strain. The most common operation mode is oscillation, where the sample is exposed to a sinusoidal stress or strain. The Q800 DMA capabilities also include creep or stress relaxation and controlled force or strain rate. The instrument allows any sample to be characterized in different deformation modes (e.g. shear, tension/compression, dual cantilever beam, 3-point bending, and single cantilever). The single cantilever configuration, as seen in Figure 2.5, was chosen for this study due to the smaller sample size required.

DMA testing consisted of running samples under the DMA multi-frequency – strain mode and temperature step frequency sweep test. The DMA multi-frequency – strain mode consists of oscillating (deforming) the sample at different frequencies under a controlled (fixed) rate of deformation (strain percent). The temperature step frequency sweep test exposes the material sample to a series of increasing isothermal temperatures. At each temperature, the material sample is deformed at a constant amplitude (strain) over a set of frequencies and the mechanical properties (modulus and energy dissipation) are measured.

Figure 2.5. TA Instruments Q800 Dynamic Mechanical Analyzer (DMA) (left) and single cantilever configuration setup with calibration sample (right).

2.2.1 DMA Sample Preparation

The effects of different sample fabrication methods were investigated to determine the role of load intensity, load frequency, and temperature on hysteretic dissipation. Samples were prepared by several methods to identify any process effects on the response of the material. The goal was to determine the simplest method of preparation that produced samples representative of manufactured thermoplastic elastomer suspension pads. The three types of sample preparations are transfer molded coupons, injection molded coupons, and coupons machined from an actual pad. The transfer molded samples were fabricated by shredding an elastomer suspension pad and then transfer molding them in a heated platen press. The resulting thin disks

were allowed to equilibrate for 36 hours and then cut into the appropriate size for DMA testing. This procedure is illustrated in Figure 2.6.

Figure 2.6. Transfer molding process for DMA sample preparation.

The second type of sample was obtained by using the injection molding process as seen in Figure 2.7. New pellets of material were molded into standard flex or tensile bars using a BOY injection molding machine. These samples were then cut to length for use in the DMA.

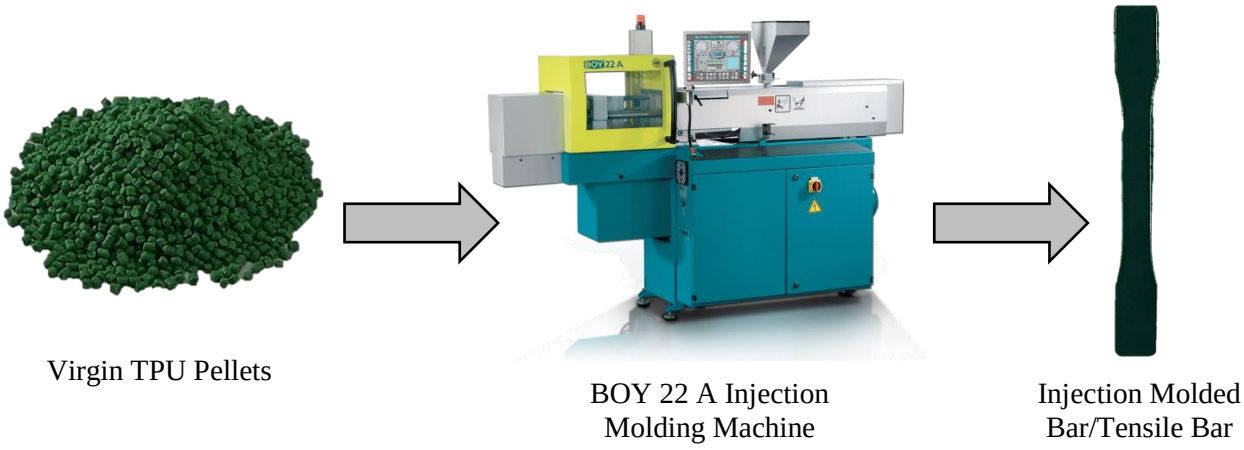

Figure 2.7. Injection molding process for DMA sample preparation.

Finally, the third type of sample was milled out from an actual elastomer suspension pad like the one shown in using a vertical band saw cutter, as shown in Figure 2.8.

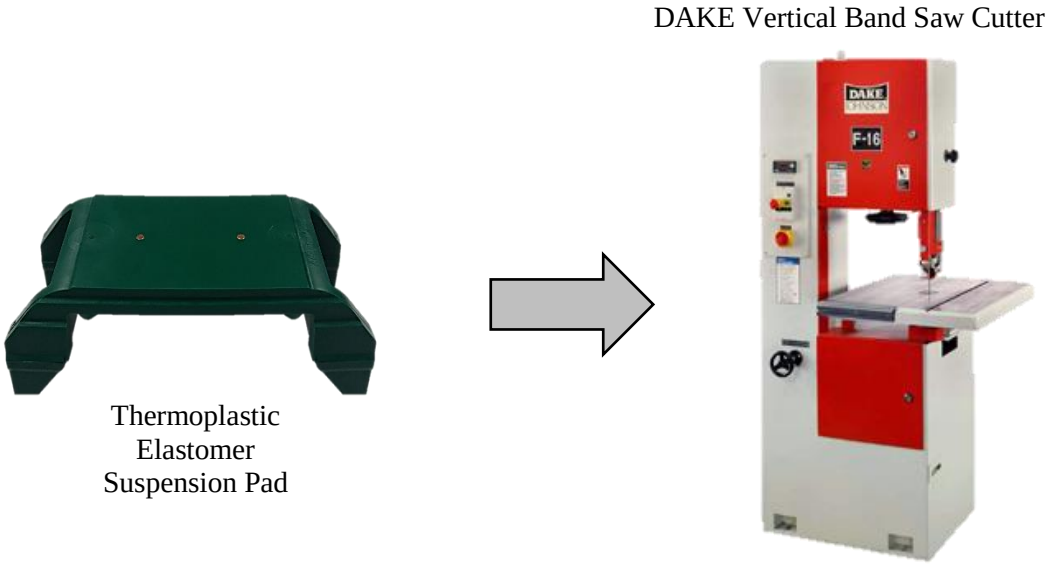

Figure 2.8. Machined pad process for DMA sample preparation.

2.2.2 Phase One Characterization

The testing in phase one consisted of equilibrating the sample at 35°C (95ºF) for 10 minutes. After that, the first frequency sweep was run. The frequency sweep subjects the sample to an oscillating load at frequencies varying from 0.1 to 100 Hertz; however, data analysis was only accounted for from 0.1 to 50 Hz. After each frequency sweep was completed, the temperature was incremented 10°C (18ºF), held for 10 minutes and then another sweep was run. The final sweep was performed at 165°C (329ºF), which is well above the maximum temperature an adapter is likely to see in service. These procedures were conducted for each of the different sample preparation samples: injection molded, transfer molded, and actual pad. Two runs were conducted for each process type to check for consistency and repeatability. Figure 2.9 summarizes the procedure described in this section.

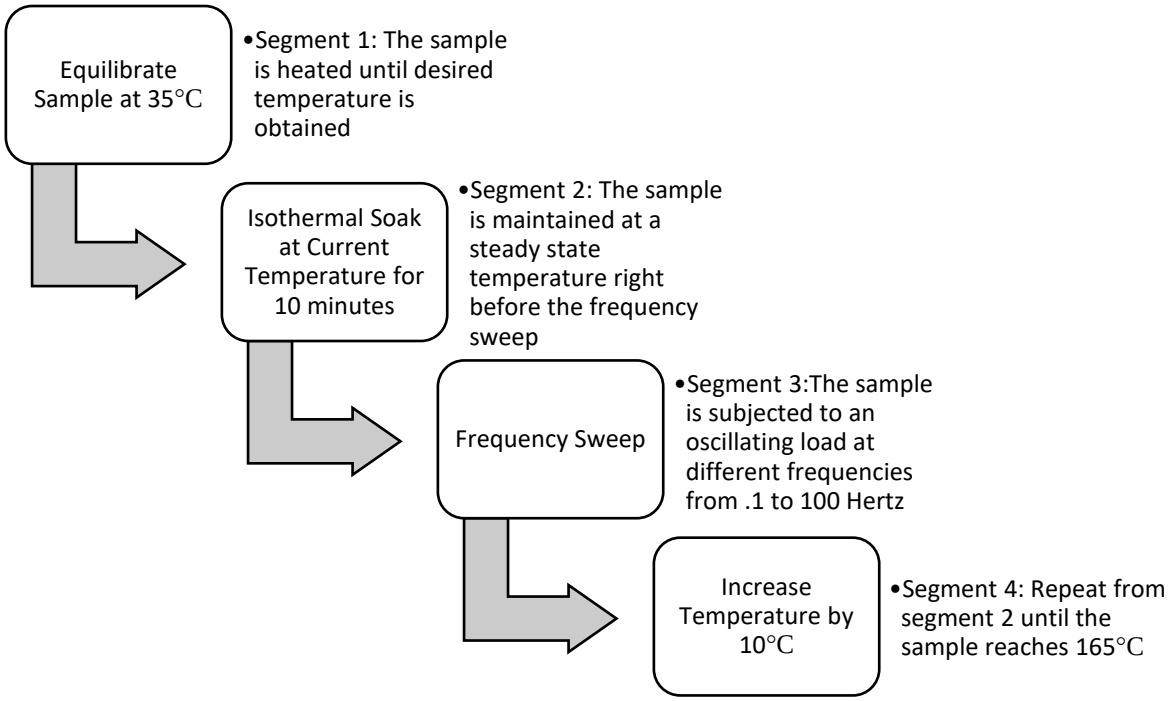

Figure 2.9. Phase one characterization DMA testing steps.

2.2.3 Phase Two Characterization

The characterization testing phase two consisted of equilibrating the sample at 30°C (86ºF) for 10 minutes. After that, the first frequency sweep was run. The frequency sweep subjects the sample to an oscillating load at frequencies varying from 0.1 to 50 Hertz. After each frequency sweep was completed, the temperature was incremented 10°C (18ºF), held for 10 minutes and then another sweep was run. The final sweep was performed at 160°C (320ºF), which is well above the maximum temperature an adapter is likely to see in service. These procedures were conducted only for the injection molded sample preparation samples since results consistently exhibited characteristics representative of manufactured pads. Four different samples were run, each at a different strain percent: 0.05%, 0.50%, 2.5%, and 12.5%; however, for the sample that was ran at 12.5% strain, the frequency range was reduced to 2 Hz due to load and displacement limitations of the software used to run DMA experiments. Multiple runs were

conducted to check for consistency and repeatability. Figure 2.10 summarizes the procedure described in this section.

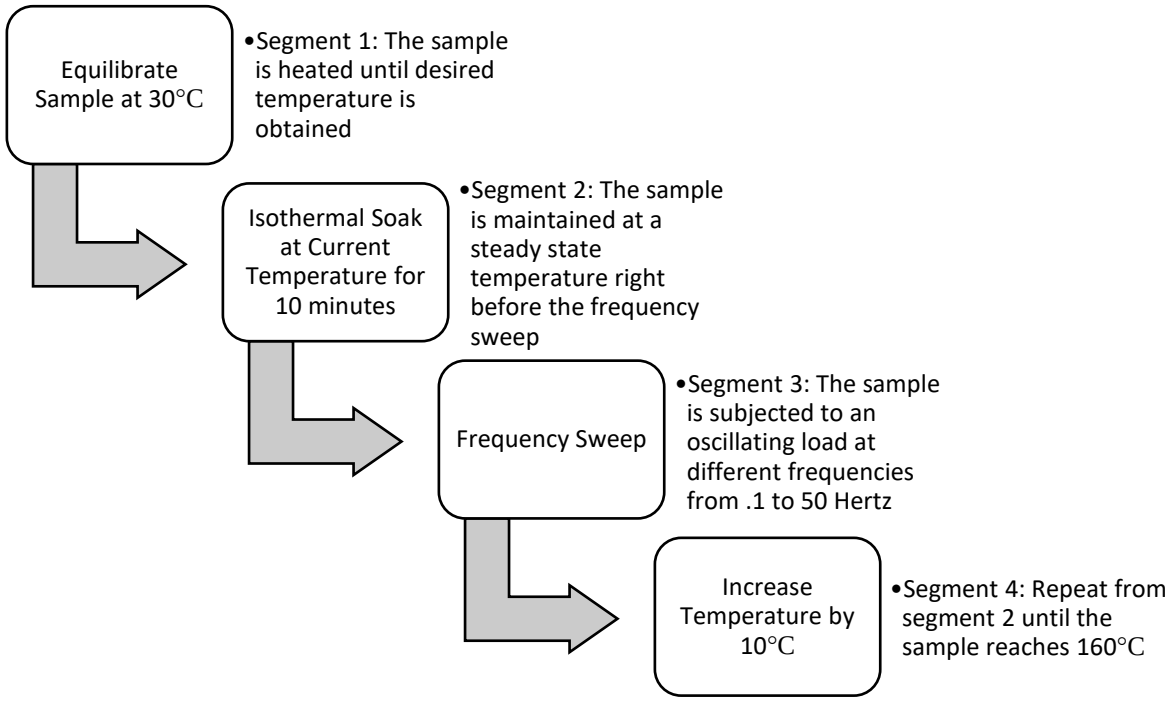

Figure 2.10. Phase two characterization DMA testing steps.

2.3 Heat Generation Quantification

The total heat generation of the material was numerically estimated using DMA data that was obtained from samples of the suspension pad material. The data showed that the loss modulus decreases as the sample temperature increases, meaning that the heat generation will be dependent on temperature and the higher the temperature of the pad the lower the dissipation of energy as heat. Since the heat generation is a function of the loss modulus, strain percent, and frequency, Eq. 1 can be used with DMA results to calculate specific power [W/m^3] dissipated at individual frequencies and temperatures.

$$P = \frac{\omega}{2}\varepsilon_A^2 E'' \qquad \text{Eq. 1}$$

Where P is the specific power in [W/m^3], ω is the frequency in [s^{-1}], ε_A is the deformation rate or strain percent in [cm/cm], and E'' is the loss modulus in [MPa]. For the heat generation calculations, the applied strain of 0.05 cm/cm in the experiments was used in conjunction with the loss modulus data obtained from the DMA tests. The heat generation is also dependent on temperature, and at each frequency, values for the internally generated heat are calculated for temperatures ranging from 30 to 160ºC (86 to 320ºF) in increments of 10ºC (18ºF). Table 2.1 and Figure 2.11 display the heat generation values for all frequency ranges as a function of temperature.

Table 2.1.Calculated heat generation values.

	50 Hz	30 Hz	20 Hz	10 Hz
Temperature [°C / °F]	Heat Generation [W/m^3]	Heat Generation [W/m^3]	Heat Generation [W/m^3]	Heat Generation [W/m^3]
30 / 86	14459	8053	4793	2070
40 / 104	10441	5842	3394	1428
50 / 122	7397	4165	2369	970
60 / 140	5065	2910	1615	641
70 / 158	3463	2068	1123	428
80 / 176	2493	1537	821	300
90 / 194	1836	1219	641	228
100 / 212	1457	1004	529	184
110 / 230	1191	859	455	155
120 / 248	1045	808	405	137
130 / 266	931	737	375	121
140 / 284	873	716	350	111
150 / 302	888	748	338	106
160 / 320	860	781	313	100

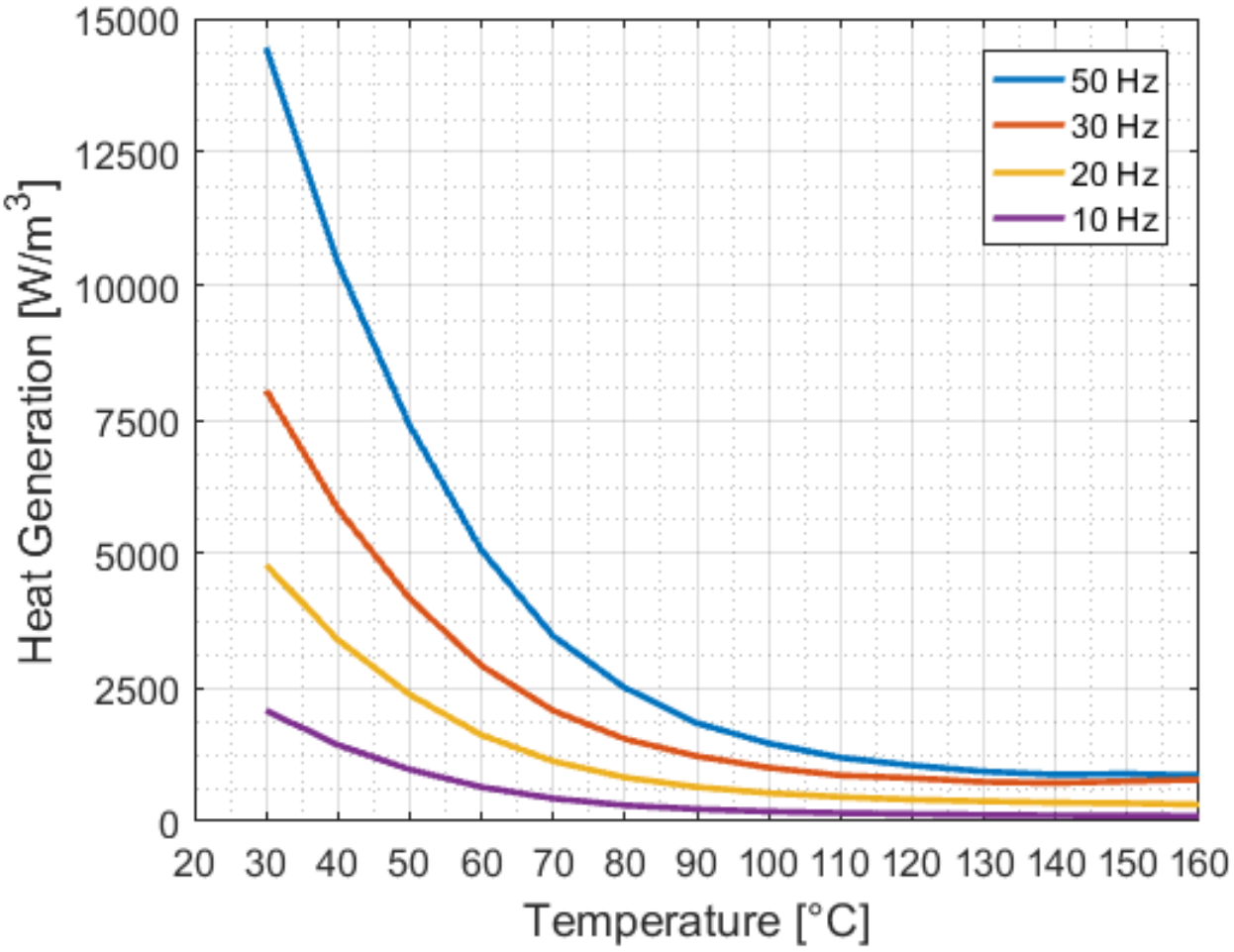

Figure 2.11. Heat generation curves at different loading frequencies.

CHAPTER III

EXPERIMENTAL METHODS AND PROCEDURES

The development of an experimentally validated finite element analysis model requires a thorough thermal analysis of the railroad tapered-roller bearing. In order to conduct the finite element analysis and compare to the experimental results, a database of the temperature histories of all the railroad tapered-roller bearings, both defective and healthy, that has been assembled by the University Transportation Center for Railway Safety (UTCRS) at the University of Texas Rio Grande valley (UTRGV) was utilized. The laboratory experiments conducted at UTRGV were performed using two dynamic bearing test rigs, a single bearing tester (SBT) and a four-bearing tester (4BT). The experimental setups were designed to recreate field service operation conditions.

3.1 Single Bearing Tester Setup

The single bearing tester is specifically designed to closely mimic railroad service conditions which a railroad bearing experiences. The single bearing tester, shown in Figure 3.1, can apply lateral (axial), impact, and vertical loads on one Class F (6½"×12") or Class K (6½"×9") tapered-roller bearing. This test rig can provide up to 22 kN (5 kips) of lateral load, a variable frequency (0-3 Hz) 70g impact load, in addition to vertical loads of up to 267 kN (60 kips) applied to a single railroad bearing. The vertical load is applied utilizing a hydraulic

cylinder capable of applying loads ranging from 0 to 175% of full load. A fully loaded railcar (100% load) corresponds to an applied load of 153 kN (34.4 kips) per bearing for Class F and Class K bearings, whereas, an empty railcar (17% load) corresponds to an applied load of 26 kN (5.85 kips) per bearing as stated in AAR standards for Class F and K bearings [4]. The single bearing tester uses a variable-speed motor powered by a variable-frequency drive (VFD), which simulates train speeds ranging from 5-137 km/h (or 8-85 mph). Forced convection cooling is achieved with two industrial strength fans, as depicted in Figure 3.2, that produce an average air stream of 18 km/h (11.2 mph). The air stream produced by the fans is meant to simulate the airflow passing across the bearing in field service.

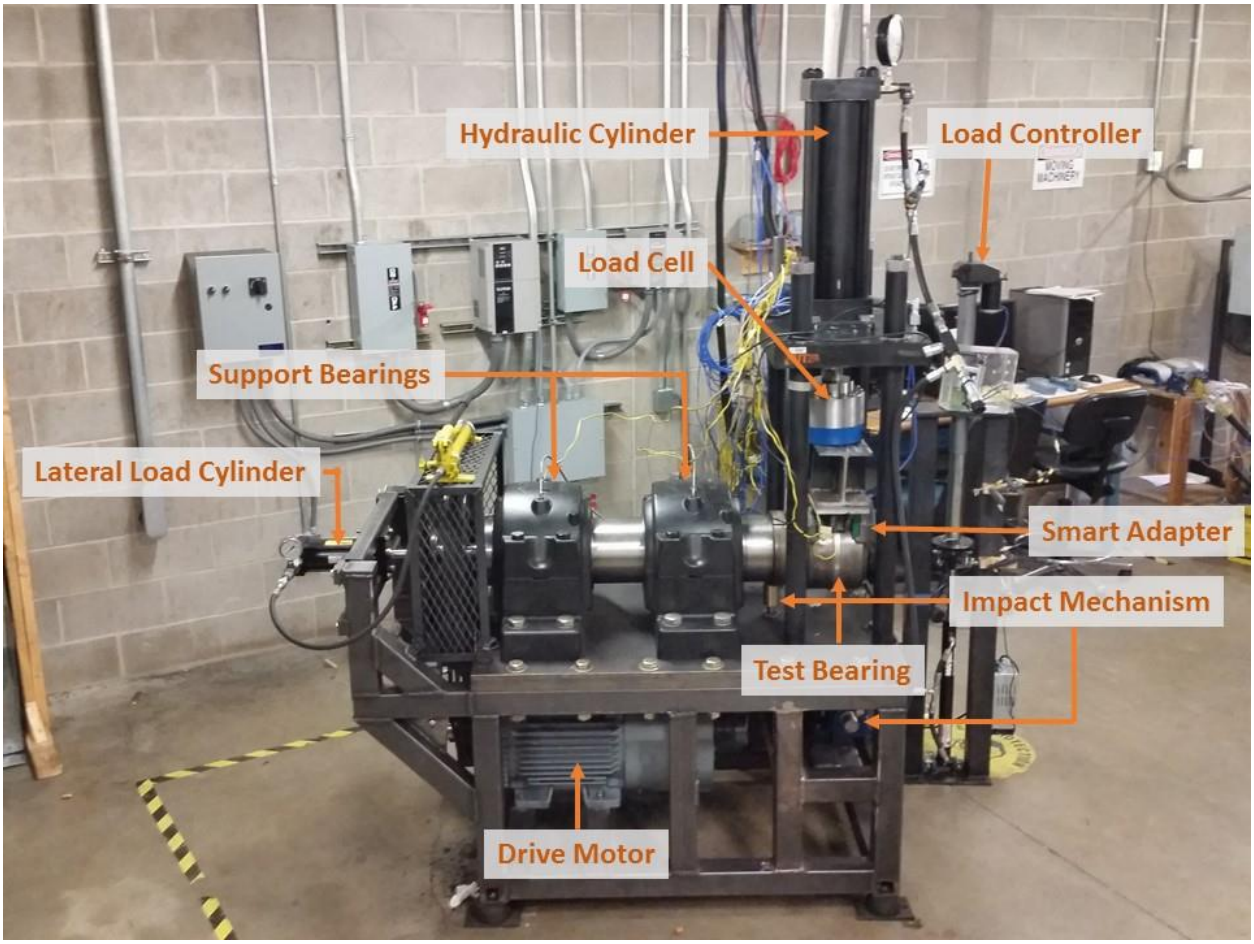

Figure 3.1. Single bearing tester (SBT) with annotations.

3.2 Four-Bearing Tester Setup

The four bearing tester (4BT), shown in Figure 3.2, accommodates four of the abovementioned tapered-roller bearings (either Class K or Class F). Each bearing tested in the laboratory is assembled using AAR (Association of American Railroads) standards. The assembled bearings are then mounted onto the test axle by means of a 300-ton hydraulic press. Following the test rig assembly, bearings were labeled B1 to B4 in ascending order from the pulley side to the end cap side (reference Figure 3.3). The 4BT can only apply vertical loads with similar ranges to those of the SBT using a similar hydraulic cylinder. The load from the hydraulic cylinder is applied directly to the two centrally located bearings, referred to as "top-loaded" bearings; the reaction load is then evenly distributed to the two outer bearings, referred to as "bottom-loaded" bearings. The four-bearing tester also uses a variable-speed motor powered by a variable-frequency drive (VFD), which simulates train speeds ranging from 5-137 km/h (or 8-85 mph). Forced convection cooling is achieved with two industrial strength fans, as depicted in Figure 3.2, that produce an average air stream of 18 km/h (11.2 mph). The air stream produced by the fans is meant to simulate the airflow passing across the bearing in field service. The four-bearing tester is enclosed within a temperature-controlled environmental chamber capable of producing ambient temperature conditions as low as -40ºC (-40ºF) and as high as 65.6ºC (150ºF).

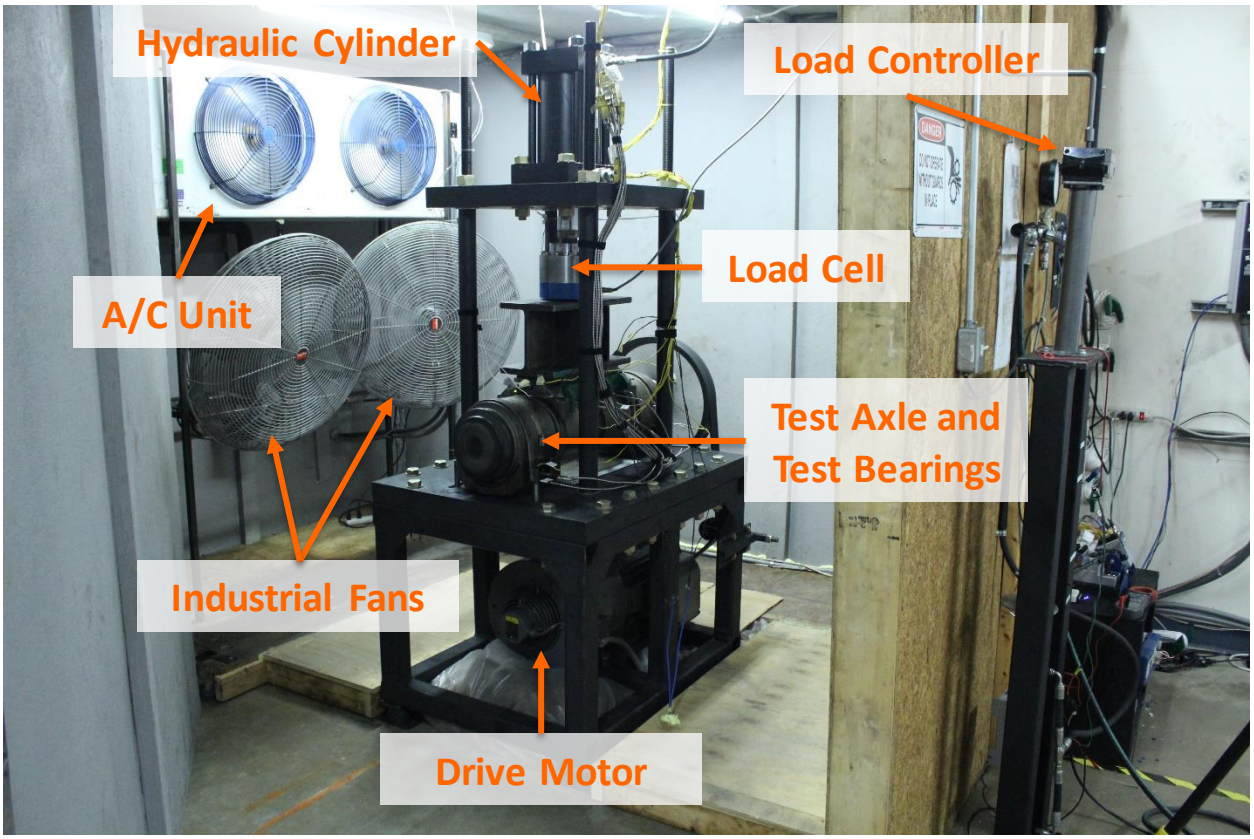

Figure 3.2. Four bearing tester (4BT) with annotations.

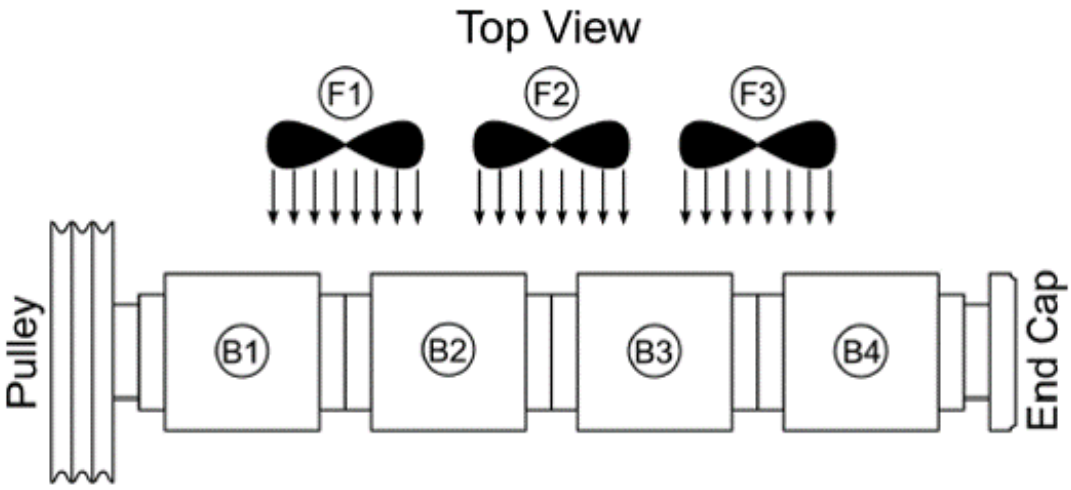

Figure 3.3. Schematic showing the top view of the four-bearing tester with test bearings labeled.

3.3 Instrumentation Setup

Both dynamic bearing test rigs are equipped with a complete set of instrumentation that collects data from the test bearings. The data is acquired by K-type thermocouples, bayonet

thermocouples, 500g high-frequency accelerometers, a high-accuracy high precision load cell, and the 70g accelerometers devised by the UTCRS research group. Data collected were recorded utilizing a National Instruments (NI) data acquisition system (DAQ) programmed using LabVIEW™. The NI PXIe-1062Q DAQ is equipped with a NI TB-2627 card to collect temperature data from the thermocouples and an 8-channel NI PXI-4472B card to record the accelerometers that were used in this study. The accelerometers were connected to the NI PXI-4472B card via 10-32 coaxial jack and a BNC connection. The data analysis was performed using the mathematical software MATLAB™.

3.3.1 Single Bearing Tester Instrumentation Setup

The test bearing is equipped with Class F or K AdapterPlus™ bearing adapter, complete with an AdapterPlus™ thermoplastic elastomer suspension pad. The adapter is machined to accept three accelerometers, a flex circuit (Smart Adapter insert) with load and temperature sensing capabilities, four bayonet thermocouples, and an adapter K-type thermocouple. Figure 3.4 indicates the accelerometer and thermocouple mounting locations on the AdapterPlus™ bearing adapter. To ensure the accuracy and reliability of the bayonet thermocouples, seven K-type thermocouples were affixed by a hose clamp along the spacer ring region of the outer ring (cup) of the test bearing. Figure 3.5 displays the placement locations of the thermocouples on the outer ring of the test bearing. In addition to the thermocouples that monitored the temperature of the test bearing within the axle assembly of the test rig, two K-type thermocouples were placed along each side of the test bearing to monitor and record the surrounding ambient temperature.

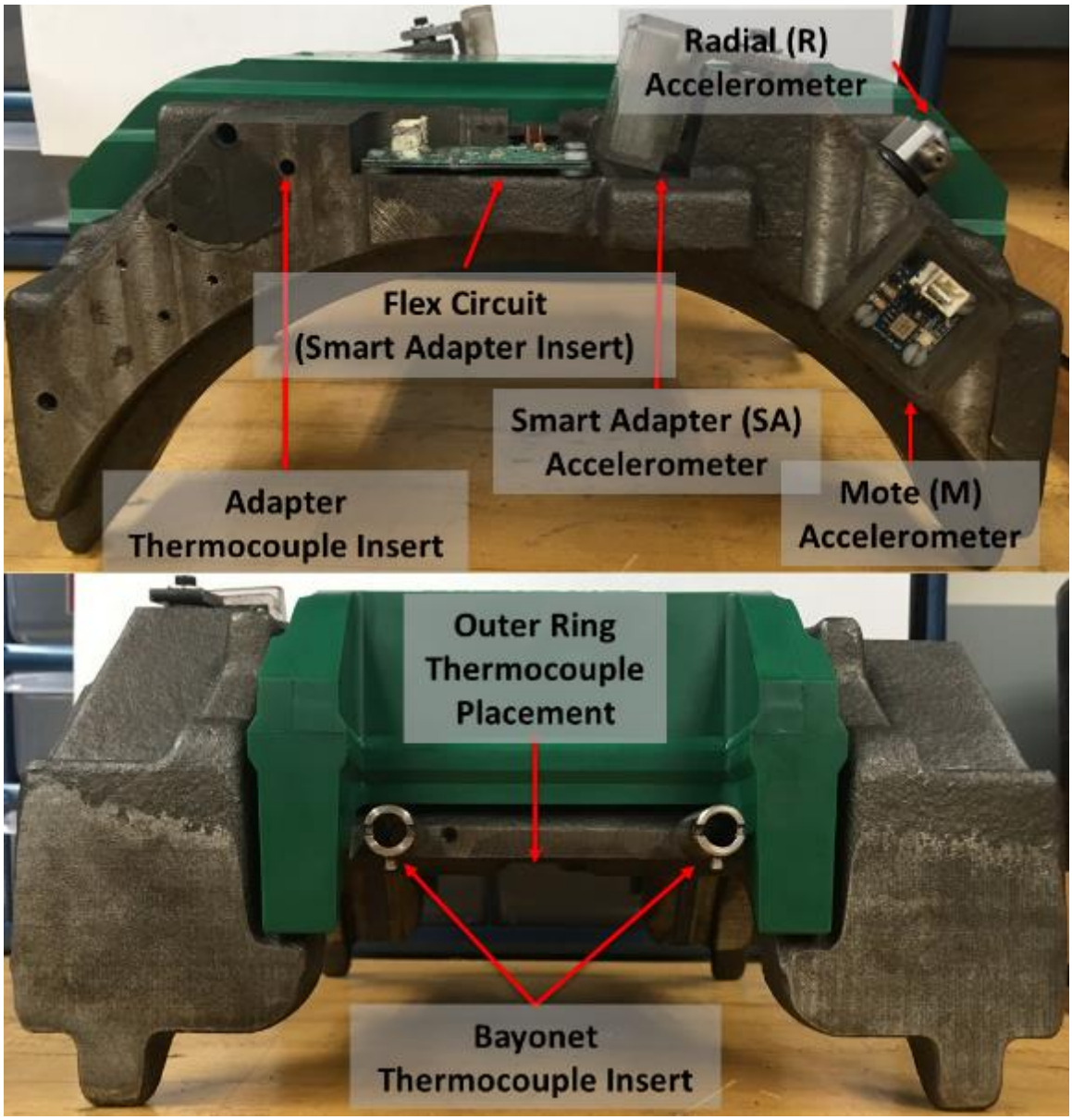

Figure 3.4. Indicated accelerometer and thermocouple mounting locations on the AdapterPlus™ bearing adapter.

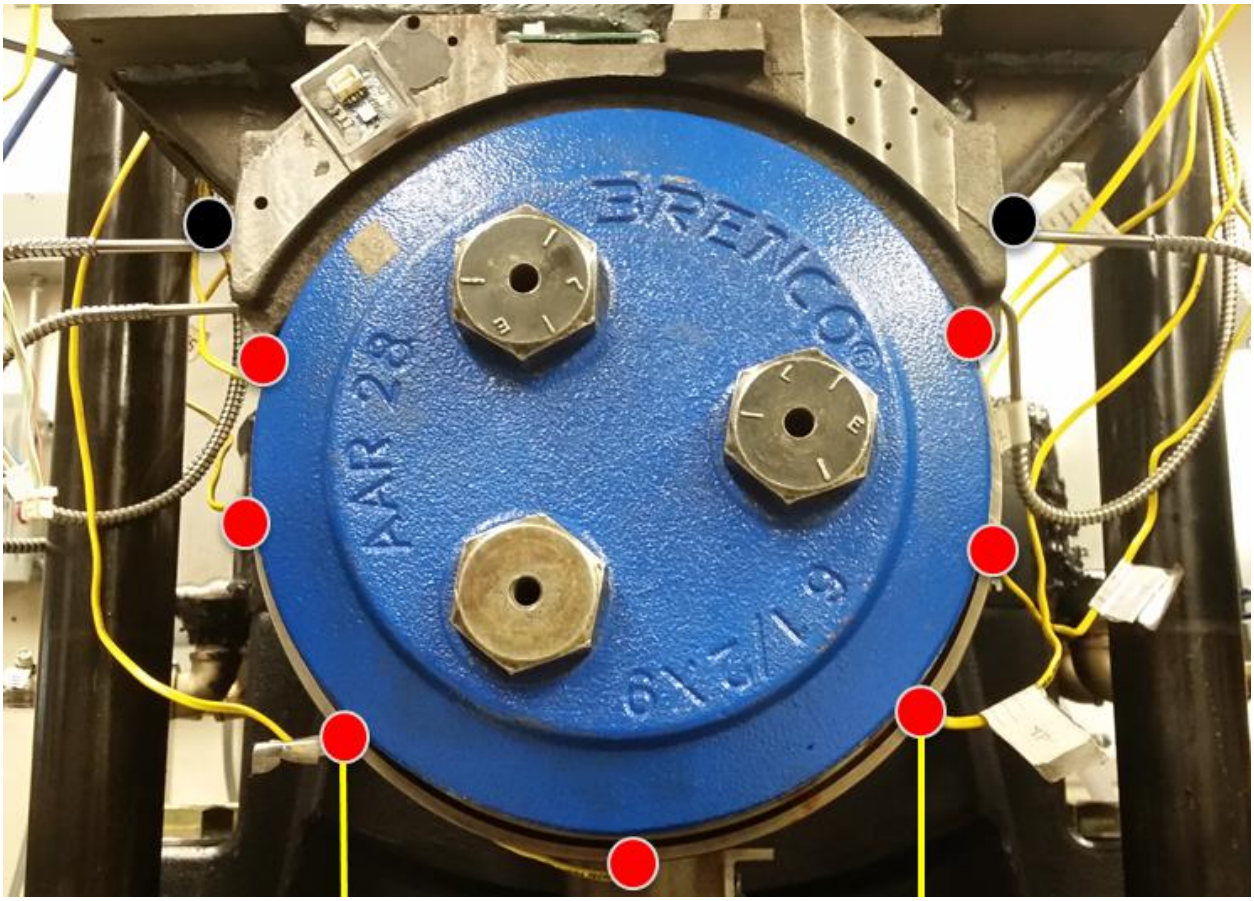

Figure 3.5. Indicated placement locations of the thermocouples on the outer ring of the test bearing (red) and on the AdapterPlus™ bearing adapter (black).

3.3.2 Four-Bearing Tester Instrumentation Setup

Each of the top-loaded bearings was equipped with a Class F or K AdapterPlus™ bearing adapter, complete with an AdapterPlus™ thermoplastic elastomer suspension pad. Similar to the instrumentation setup of the single bearing tester, the adapters are machined to house three accelerometers, a flex circuit (Smart Adapter insert) with load and temperature sensing capabilities, two bayonet thermocouples, and an adapter K-type thermocouple. Bottom-loaded bearings rested on all-steel adapters, machined to house two bayonets, and two accelerometers. The thermocouple and accelerometer placement locations on the AdapterPlus™ bearing adapter are similar to those of the single bearing tester (reference Figure 3.4). Each bayonet thermocouple was centered on each of the two outer ring (cup) raceways to measure the

temperature produced by each raceway. To ensure the accuracy and reliability of the bayonet thermocouples, one K-type thermocouple was affixed to the center of each bearing cup by a hose clamp aligned between the two bayonets. In addition to the thermocouples that monitored the temperatures of the four test bearings within the axle assembly of the test rig, two K-type thermocouples were placed along each side of the test axle to monitor and record the surrounding ambient temperature. A total of sixteen K-type thermocouples were employed to monitor and record the temperatures of the four-bearing test rig experimental setup.

3.4 Laboratory Test Conditions

Field conditions were recreated in a laboratory setting utilizing both dynamic bearing test rigs. Tests included a combination of defect-free (healthy or control) and defective Class F/K bearings run at various speeds and loads. Table 3.1 and Table 3.2 display the laboratory operation condition loads and speeds, respectively. Table 3.3 displays the laboratory conditions that were labeled as normal and abnormal operation conditions for FEA data comparison.

Table 3.1. Laboratory operation condition loads.

Class F and K	17% of Full Load	100% of Full Load
Force [kN / kips]	26 / 5.85	153 / 34.4

Table 3.2. Laboratory operation condition speeds.

Train Speed [km/h] /[mph]	40 / 25	48 / 30	56 / 35	64 / 40	72 / 45	85 / 53	97 / 60	106 / 66	121 / 75	137 / 85
Rotational Speed [rpm]	234	280	327	374	420	498	560	618	700	796

Table 3.3. Laboratory operation conditions for FEA comparison.

Operation Condition	**Ambient Temperature [°C / °F]**	**Load [%]**	**Train Speed [km/h] / [mph]**
Normal	25 / 77	100	96.6 / 60
Abnormal	45 / 113	100	137 / 85

CHAPTER IV

FINITE ELEMENT MODELING AND ANALYSIS

A computer aided design (CAD) model was created and constructed in Solid Works™, which was then imported into ALGOR 20.3™ to create a finite element (FE) model to conduct heat transfer analysis. In order to determine if the heat generation values that were calculated are reasonable (reference Table 2.1), preliminary finite element modeling and analysis was performed on a model of the laboratory sample that was used for the hysteresis heating tests discussed in Chapter 2. Subsequently, the validated heat generation values were used in the finite element analysis (FEA) models of the suspension pad, and for the laboratory test rig bearing assembly.

4.1 Hysteresis Heating Test Sample Finite Element Analysis (FEA)

The finite element (FE) model of the hysteresis heating test sample is illustrated in Figure 4.1. FEA of the laboratory hysteresis heating test sample was run in order to determine if the heat generation values that were numerically estimated from the data obtained by DMA (reference Chapter 2) are reasonable. Both, the steady state and the transient response analyses at different time periods were acquired in order to replicate the results from the laboratory hysteresis heating tests. The boundary conditions applied were convection load on the circumference lateral area, heat generation though out the model, and ambient temperature. Please note that in the following simulations, no heat transfer was allowed in the top and bottom surfaces of the cylindrical model

(i.e. insulated surfaces). Different sensitivity analyses were run to study the dependence of the results on the boundary conditions that were applied to validate the laboratory experiments. The volume heat generation was applied as a constant and temperature dependent boundary condition. For the convection coefficient, there is a broad range of values that can be selected; however, a sensitivity analysis was conducted on different convection coefficient values within the range of the free convection values for air. For the initial finite element analysis, an overall convection coefficient of 5 $W \cdot m^{-2} \cdot K^{-1}$ was selected and an ambient temperature of 23.1ºC was used. Material properties were sourced from BASF literature TPU using data from grades with the same shore durometer value. A thermal conductivity of 0.25 $W \cdot m^{-1} \cdot K^{-1}$ along with a mass density of 1160 $kg \cdot m^{-3}$ and a specific heat of 2.3 $J \cdot g^{-1} \cdot K^{-1}$ were selected as the specific properties.

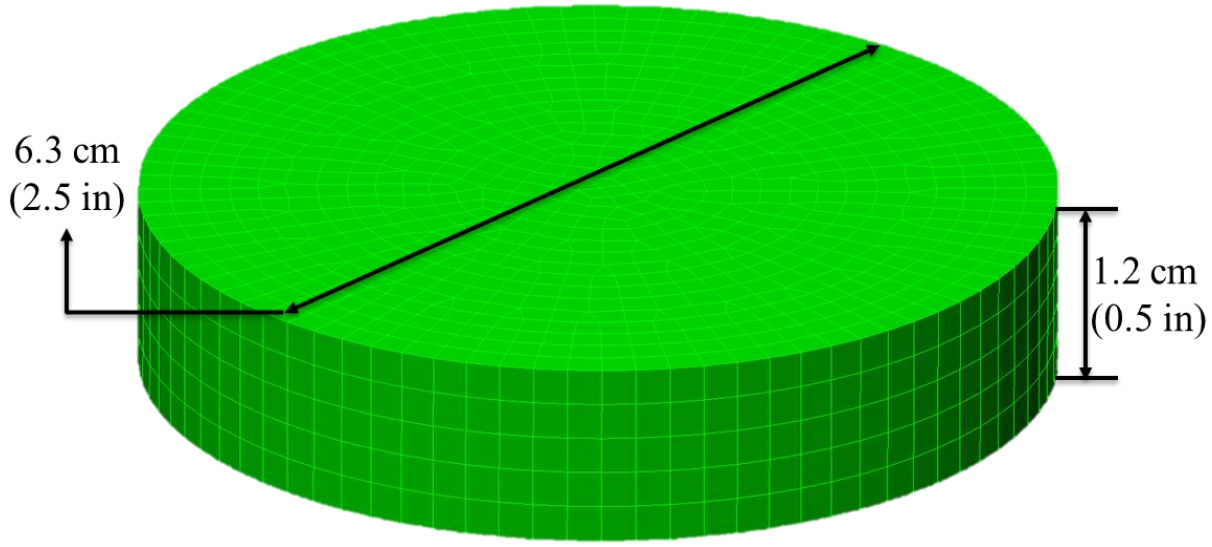

Figure 4.1. Hysteresis heating test sample FE model.

First, in order to have reliable results, a sensitivity analysis on the mesh size of the model was run in order to determine whether or not there is convergence of the FEA results. Decreasing the mesh size increases the number of elements and nodes in the model changing the final result

every time until the result is similar to that of the exact solution [9]. In essence, the steady-state temperature analysis was used to run the model at different mesh sizes from 100% down to 25% of the original mesh size to compare the resulting temperature. After ensuring convergence of the model, a mesh size of 75% of the original mesh size was selected using brick elements, which resulted in 7721 total elements. To reduce the number of elements, symmetry was taken into consideration, where half of the sample was used, and later, only quarter of the test sample was used. Another sensitivity analysis on the mesh size was run for each symmetric model, and convergence was checked and verified.

Table 4.1 summarizes the results of the steady-state temperature of the cylindrical test sample with an applied heat generation produced by a 20 Hz cyclic loading. The results show that the use of a constant or temperature dependent heat generation model yield the same equilibrium temperature. Both equilibrium temperatures show a similar increase above ambient representative of the approximately 5°C measured in the laboratory (reference Figure 2.2). In addition, the time it takes to reach the steady-state temperature is approximately the same for both the constant and temperature dependent heat generation models. Since the steady state temperature is below 30°C, the FEA of the temperature dependent model only applies the 30°C heat generation value, which is the same value used in the constant heat generation model. It can be said that the effect of the temperature dependent heat generation does not impact the model for low cyclic loading frequencies such as 20 Hz.

Table 4.1. Steady-state temperature and time of laboratory test sample FE model with an applied heat generation produced by a 20 Hz cyclic loading.

Heat Generation	Time [min]	Temperature [°C / °F]
Constant	~55	28.05 / 82.49
Temperature Dependent	~55	28.05 / 82.49

To test for reliability, finite element analysis was conducted using the same test sample now with an applied heat generation produced by a 50 Hz cyclic loading. Table 4.2 presents the results that exhibit a trend where the constant heat generation case predicts a higher equilibrium temperature. In this case, it takes approximately 25% less time for the temperature to reach steady state using the constant heat generation model. The latter is due to the reduced amount of energy that is being generated at a specific temperature for the temperature dependent heat generation model.

Table 4.2. Steady-state temperature and time of laboratory test sample FE model with an applied heat generation produced by a 50 Hz cyclic loading.

Heat Generation	Time [min]	Temperature [°C / °F]
Constant	~46	35.79 / 96.42
Temperature Dependent	~60	35.6 / 96.1

Figure 4.2 displays the temperature map of the hysteresis heating test sample with plots of both loading frequencies: 20 and 50 Hz. The figure indicates that the highest temperature is in the center of the cylindrical test sample, and when applying symmetry, it can be seen that the peak temperature is located in the center-middle point of the cylindrical test sample. The center-middle point of the test sample is the location where temperature measurements were taken during laboratory testing.

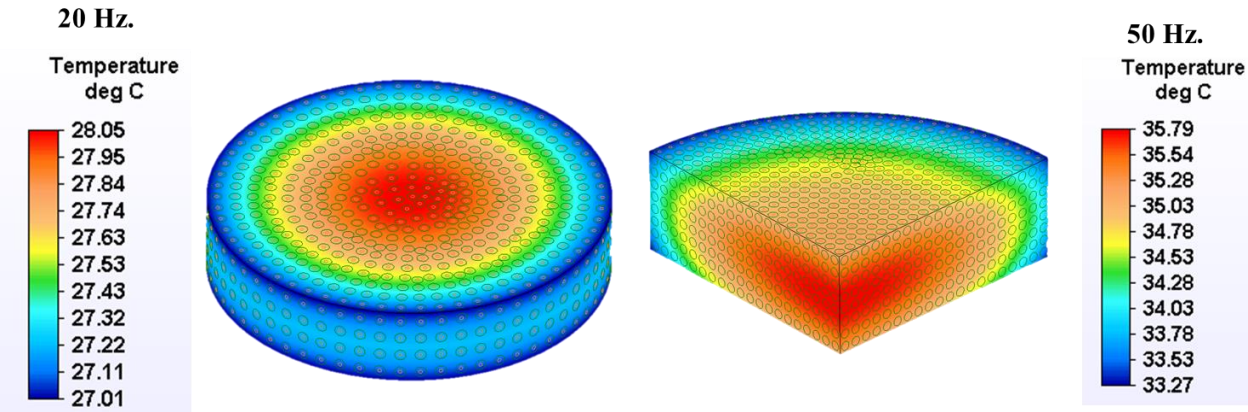

Figure 4.2. Temperature map of steady-state analysis of full cylindrical sample (left) and quarter symmetrical cylindrical sample (right) at frequency loadings of 20 Hz and 50 Hz.

4.2 Thermoplastic Elastomer Suspension Pad Finite Element Analysis (FEA)

Once the hysteresis heating test data was validated, and the heat generation values that were calculated from the data obtained by DMA were found to be reasonable, it was time to conduct FEA analysis on the thermoplastic elastomer suspension pad. The main goal is to analyze the effect of the heat generation due to the hysteresis heating of the suspension pad on the temperature distribution of the pad, and to obtain the temperature distribution maps resulting from different operation conditions.

From previous studies conducted on the thermoplastic elastomer steering pad, it is known that most of the heat from the bearing adapter is conducted to the central square area on the bottom side of the adapter pad [4]. The FE model used is the same as the one used in reference [4]. Sensitivity analyses were carried out to study the dependence of the results on boundary conditions and material properties including elastomer thermal conductivity. Figure 4.3 displays the FE model of the steering pad used for the different analyses performed fir this study. A mesh size of 75% was used, and the brick element type was selected. The final meshed model consisted of 5248 total elements.

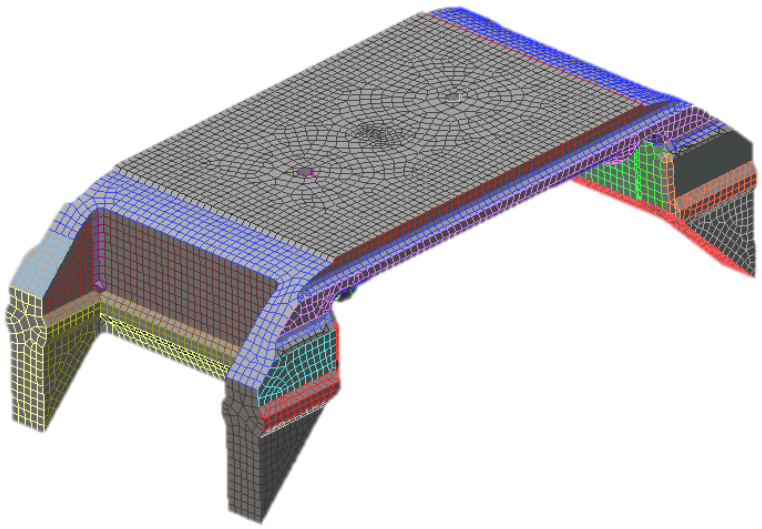

Figure 4.3. FE model of thermoplastic elastomer suspension pad

Figure 2.11 clearly demonstrates that the internally generated heat decreases when temperature increases. Using the model illustrated in Figure 4.3, transient state analysis was conducted for a period of 12 hours. The latter was done in order to represent operation conditions in service during typical running times. A thermal conductivity of 0.25 $W \cdot m^{-1} \cdot K^{-1}$ along with a mass density of 1160 $kg \cdot m^{-3}$ and a specific heat of 2.3 $J \cdot g^{-1} \cdot K^{-1}$ were selected as the specific properties. An average convection coefficient of the pad can be obtained with a minimum airflow of 5 $m \cdot s^{-1}$, as calculated in previous studies [4]. This convection coefficient is only applied to those areas completely exposed to the air, and not the top and bottom surfaces that are in direct contact with other components [4]. The applied boundary conditions are: a convection coefficient of 17.9 $W \cdot m^{-2} \cdot K^{-1}$, temperature-dependent heat generation due to a loading frequency of 50 Hz, and an ambient temperature for both normal and abnormal operation conditions. Please note that in the following simulations, no heat transfer was allowed in the top and bottom surfaces of the cylindrical model (i.e. insulated surfaces). The obtained top and bottom surface temperatures were both used as reference temperatures to compare with previous studies [4]. For example, the temperature map of the thermoplastic elastomer suspension pad was obtained for

normal operation conditions from previous studies [4]. The study concluded that the bottom surface of the suspension pad conducts most of the heat from the adapter, reaching a temperature of about 50ºC (122ºF). However, for these FEA simulations (assuming no heat transfer to railcar), heat transfer will not flow from the pad to the adapter since the steering pad temperature increases to more than 50ºC as observed in the following results.

Figure 4.4 shows the temperature distribution map during normal operation. The results show that when a temperature dependent heat generation value and ambient temperature of 23.1ºC (73.6ºF) are applied, the peak temperature of the pad reaches 62ºC (143.6ºF). The peak temperature location is at the center-middle area of the suspension pad.

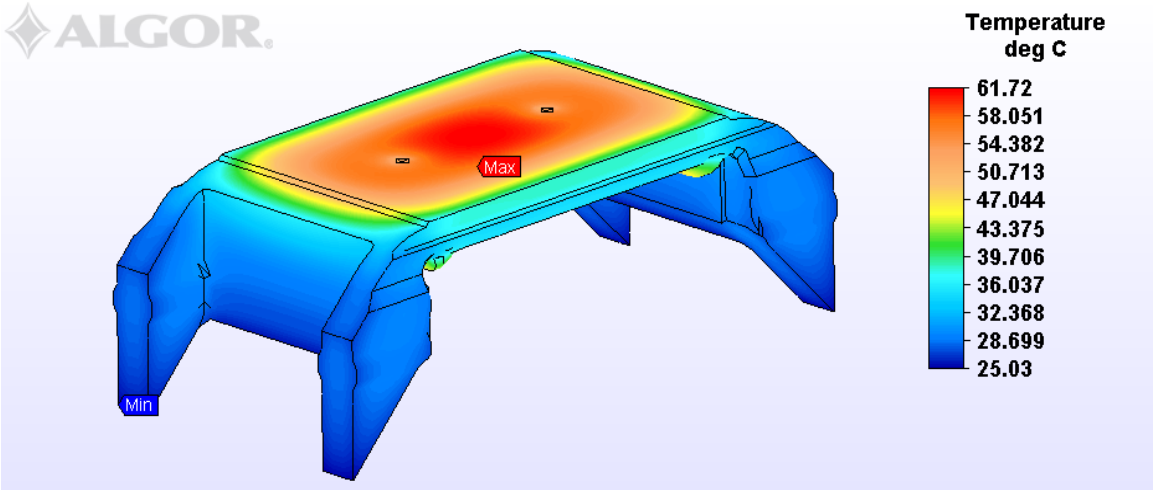

Figure 4.4. Temperature map of thermoplastic elastomer suspension pad FE model subjected to normal boundary conditions.

Now, when abnormal boundary conditions, such as an ambient temperature of 45ºC (113ºF) is applied, it can be seen from Figure 4.5 that the absolute temperature of the pad is significantly higher. This could mean that the heat generation does have a significant impact on the temperature of the suspension pad, which may compromise the structural integrity of the pad over 12 hours of harsh operation conditions.

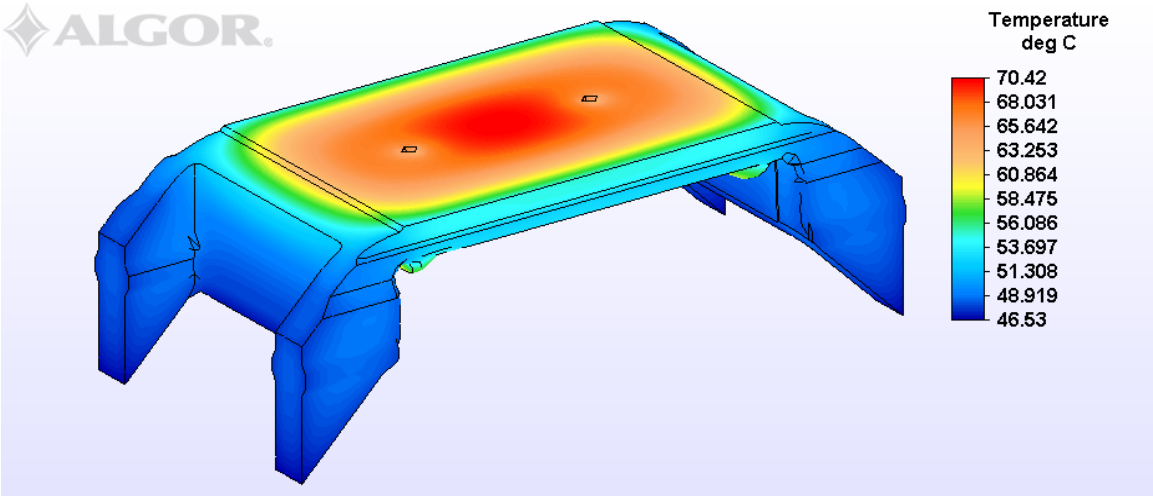

Figure 4.5. Temperature map of thermoplastic elastomer suspension pad FE model subjected to abnormal boundary conditions.

Further scenarios, such as applying a constant heat generation value under steady state analysis, were studied. Figure 4.6 shows the resulting temperature map of one of these scenarios. An ambient temperature of 45ºC (113ºF), and a constant heat generation value due to a frequency loading of 50 Hz were applied as the boundary conditions. The peak temperature of the suspension pad under the aforementioned conditions is approximately 137ºC (278.6ºF), which is clearly above the softening temperature of the pad material (i.e. 120ºC or 248ºF).

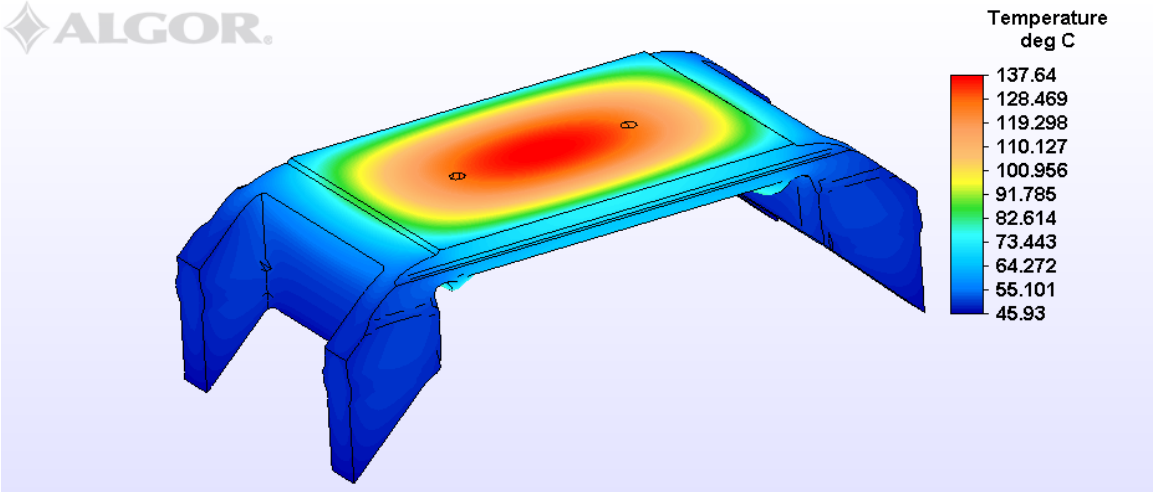

Figure 4.6. Temperature map of thermoplastic elastomer suspension pad FE model subjected to worst-case scenario boundary conditions.

4.3 Laboratory Test Rig Bearing Assembly Finite Element Analysis (FEA)

The final step was to investigate the effect of the heat generation due to the hysteresis heating of the suspension pad on the thermal management of the railroad tapered-roller bearing. This section presents an experimentally validated finite element thermal model, depicted in Figure 4.7, that can be used to obtain temperature distribution maps of complete bearing assemblies in service conditions.

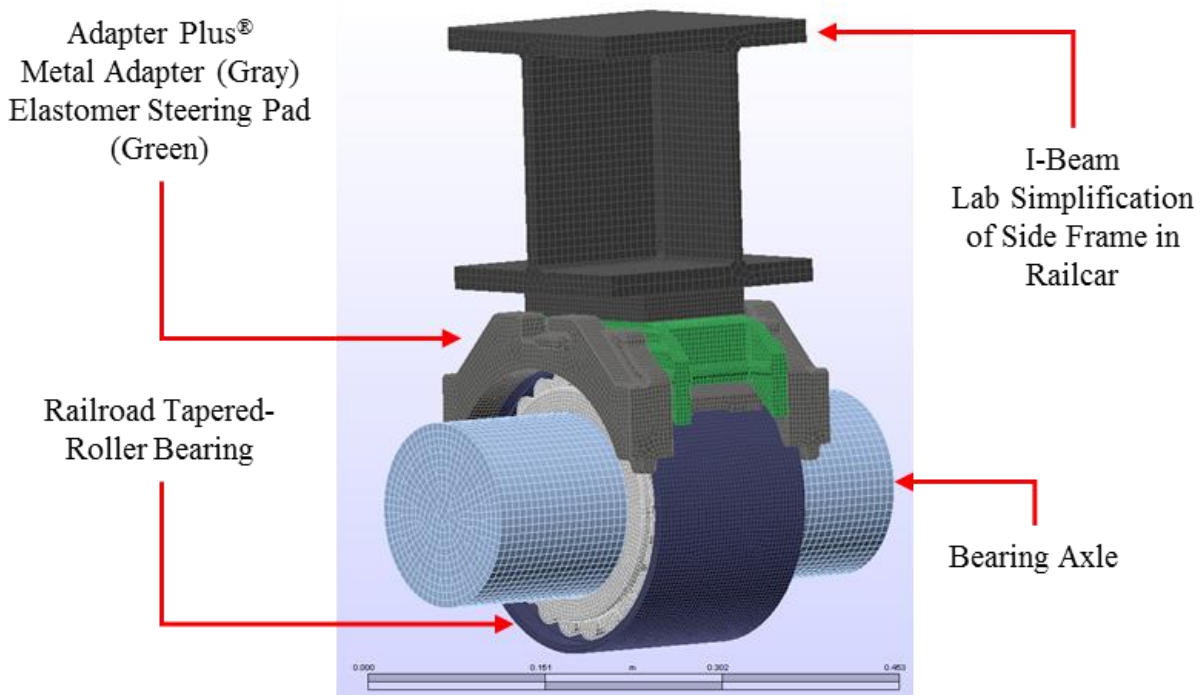

Figure 4.7. Laboratory bearing assembly test rig FE model.

4.3.1 FEA Modeling of Laboratory Test Rig Bearing Assembly

A combination of bricks, wedges, pyramids, and tetrahedral elements were used to successfully mesh the complete model. The complete laboratory bearing assembly FE model includes a tapered-roller bearing that is pressed onto an axle and assumes that all rollers contribute the same amount of thermal load. The length of the axle accounts for the different thermal runways caused by the insulating properties of the thermoplastic elastomer suspension pad. Some of the boundary conditions as well as the overall heat transfer coefficients were

acquired from experimental and theoretical work performed previously and summarized in reference [3]. Four major boundary conditions were applied: conduction, convection, heat flux, and heat generation. Model simplifications were made including the following: no roller cages, seals, wear rings, or grease were included. The thermal resistances of both the grease and the polyamide cages are very large compared to that of the other bearing components, and their exclusion is justified in reference [2]. Other assumptions include the contact area of the roller to the cup (outer ring) and cone (inner ring) raceways and the thermal contact resistance between the bearing cup and the adapter. Since the roller-cone and roller-cup contact areas change whenever the bearing is loaded or unloaded, and during normal operation conditions only the upper hemisphere of the bearing is loaded, so larger contact areas exist in this region. Hence, an average value for the roller-cup and roller-cone contact area was applied to each one of the 46 rollers in the bearing assembly [2]. It is important to note that, since this is a static model, the actual rotation of the cone assemblies inside the bearing was not directly simulated, but was taken into account by applying an average heat flux through all 46 rollers in the bearing [4].

Material properties for the bearing components, axle, I-beam, spacer ring, adapter, and spacer plate were all directly selected from ALGOR 20.3™. For the bearing components, AISI 8620 steel with a thermal conductivity of 49.3 $W \cdot m^{-1} \cdot K^{-1}$ was used; for the axle, I-beam, spacer ring, and spacer plate, AISI 1050 steel with a thermal conductivity of 51.9 $W \cdot m^{-1} \cdot K^{-1}$ was used, further detailed descriptions are provided in reference [4]. For the adapter pad, material properties were sourced from BASF literature on thermoplastic polyurethane (TPU) using data from material grades with the same shore durometer value. A thermal conductivity of 0.25 $W \cdot m^{-1} \cdot K^{-1}$ along with a mass density of 1160 $kg \cdot m^{-3}$ and a specific heat of 2.3 $J \cdot g^{-1} \cdot K^{-1}$ were selected as the specific properties. Ductile (nodular) iron with a thermal conductivity of

34.4 $W \cdot m^{-1} \cdot K^{-1}$ was used for the bearing adapter material. Table 4.3 obtained from reference [4] lists the convection coefficient values for all the FE model components.

Table 4.3. Convection coefficient values for each FE model component.

Part	h_{avg} [$W \cdot m^{-2} \cdot K^{-1}$]
I-beam	19.0
Spacer Plate	18.3
AdapterPlus™	17.9
Adapter Pad	17.9
Overall Average	18.1

The convection boundary condition for the bearing cup was obtained from previous theoretical and experimental work presented in references [2] and [3]. An overall heat transfer coefficient $H_o = 8.32\ W \cdot K^{-1}$ is provided for the bearing cup, taking into account the forced convection that is generated by the average air flow of 5 m/s and radiation to the ambient air at a temperature of 25ºC. However, the software appropriate units require the aforementioned convection value to be divided by the bearing cup outside surface area ($A_{cup} = 0.1262\ m^2$), leading to a cup convection coefficient $h_o = 65.9\ W \cdot m^{-2} \cdot K^{-1}$.

For the axle, the convection coefficient was obtained by using the Nusselt number correlation for a cylinder in cross-flow. A resulting value of $h_{axle} = 25\ W \cdot m^{-2} \cdot K^{-1}$ is obtained from reference [4]. For the adapter, adapter pad, I-beam, and spacer plate, the convection coefficient values were obtained by using the Nusselt number correlation for a flat plate in parallel flow.

The work reported in reference [2] indicates that the total heat input from all 46 rollers within the railroad bearing assembly is about 529 W per bearing for normal operation conditions, and 980 W for abnormal operation conditions. For simplicity, the heat flux was only applied to the surface of the rollers; i.e. 11.5 W per roller for normal operation, and 21.3 W per roller for

abnormal operation. Here, it is assumed that the rollers are the source of heat within the bearing, which is justified considering the mass of the roller (0.145 kg) relative to the mass of the bearing cup (11.53 kg) and cone (3.9 kg). Since the mass of the roller is very small compared to the mass of the cup and cone, it is safe to assume that it will heat at a much faster rate than the other two components, thus, becoming the heat source [2].

Another heat source or thermal mechanism boundary condition is the hysteresis heat generation that is produced by the thermoplastic elastomer suspension element. It was shown earlier in this chapter that an applied constant heat generation at high loading frequencies such as 50 Hz in combination with high ambient temperatures and no thermal runway can propel elastomer suspension pad temperatures significantly above the softening temperature of the pad material (i.e. 120ºC or 248ºF) [10]. The heat generation applied to the adapter pad is a constant heat generation for frequency loadings of 10 and 50 Hz, which simulate a defect-free (healthy) and defective bearing assembly in the laboratory, respectively. The heat generation is applied to both normal and abnormal condition models.

Thermal contact resistance between the adapter and bearing cup may significantly affect the amount of heat transferred to the bearing adapter. Values for the contact resistance were obtained as a result of a pressure film study explained in reference [4]. A thermal contact resistance of 0.0055 $m^2 \cdot K \cdot W^{-1}$ was applied in between the bearing cup and adapter. Consequently, in order to model both heat sources simultaneously (i.e. the heat flux of the rollers and the heat generation within the suspension pad), a thermal contact resistance of 0.01 $m^2 \cdot K \cdot W^{-1}$ was applied between the suspension pad and the metal adapter, and between the suspension pad and the I-beam spacer plate. The value for the thermal contact resistance applied between the suspension pad and the metal adapter, and between the suspension pad and the

I-beam spacer plate was obtained as the result of an optimization study conducted to match the experimentally acquired temperatures to the numerically obtained FEA results. Figure 4.8 displays the complete FE model with the convection and heat flux boundary conditions applied to each individual component.

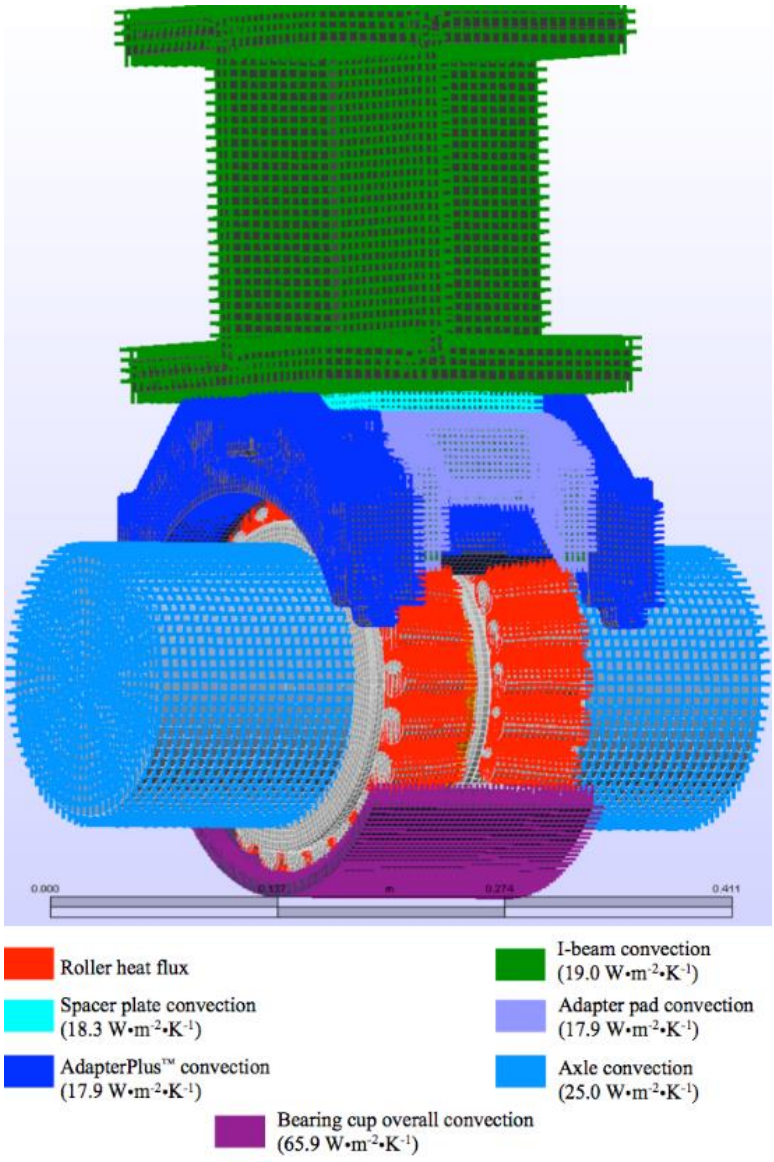

Figure 4.8. Boundary conditions applied to each FE model component.

4.3.2 FEA Validation of Laboratory Results

The finite element (FE) model thermal maps presented in reference [4] were used as the basis for the thermal maps presented in this thesis. The initial step was to replicate the experimental results presented in reference [4]. Figure 4.9 displays the FE model with markers showing the location of the selected nodes. The same reference temperature locations on the adapter were used for comparison and model validation. Using the boundary conditions and modeling methods explained in the previous section and summarized in Figure 4.8, the preliminary results shown in Figure 4.10 were obtained. A temperature map of the complete bearing assembly for normal operation conditions, displayed in Figure 4.10, was obtained as a result of the thermal finite element analysis (FEA) conducted utilizing the newly developed FE model. Table 4.4 provides a comparison between the results of the simulation of Figure 4.10 and the experimental temperature data acquired through dynamic testing. The comparison indicates a maximum temperature difference of no more than 9.5% in the thermocouple location indicated on the adapter of Figure 4.9. In the bayonet locations, the average temperature difference was only about 2%. This small difference demonstrates the efficacy of the model, and validates all of the assumptions and boundary conditions that were used to devise this new FE model. Once it was determined that the results of the complete FE model developed for this study matched the experimental results acquired from reference [4], a second simulation scenario was modeled with the inclusion of the heat generation produced by the thermoplastic elastomer suspension pad.

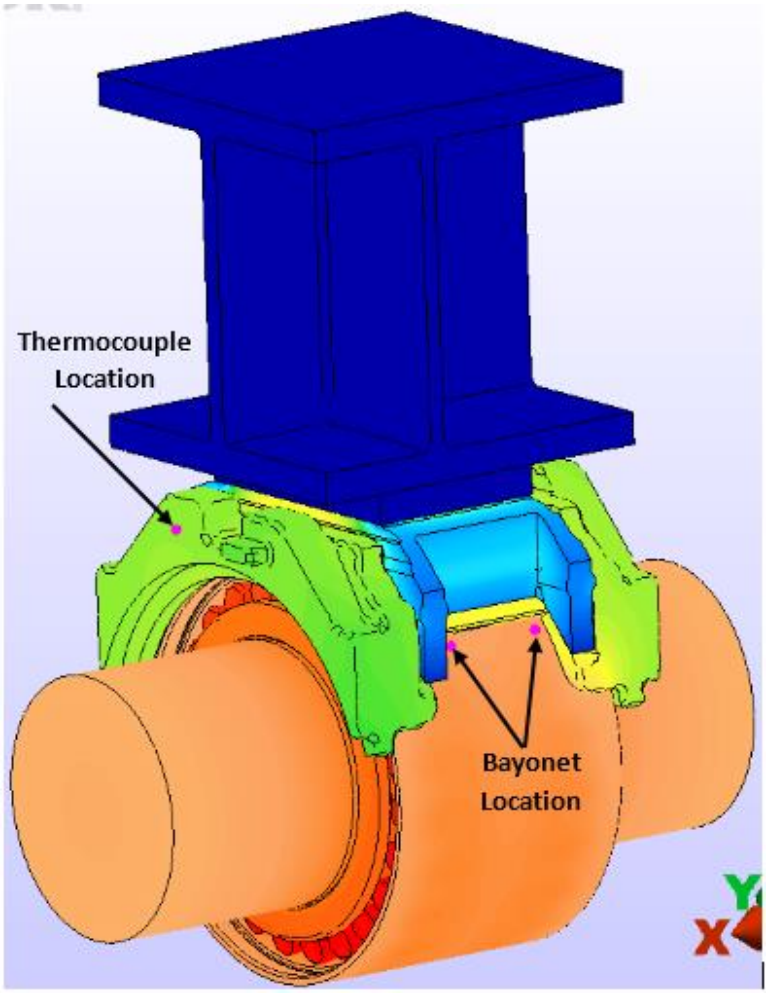

Figure 4.9. AdapterPlus™ FE model with nodes of interest indicated.

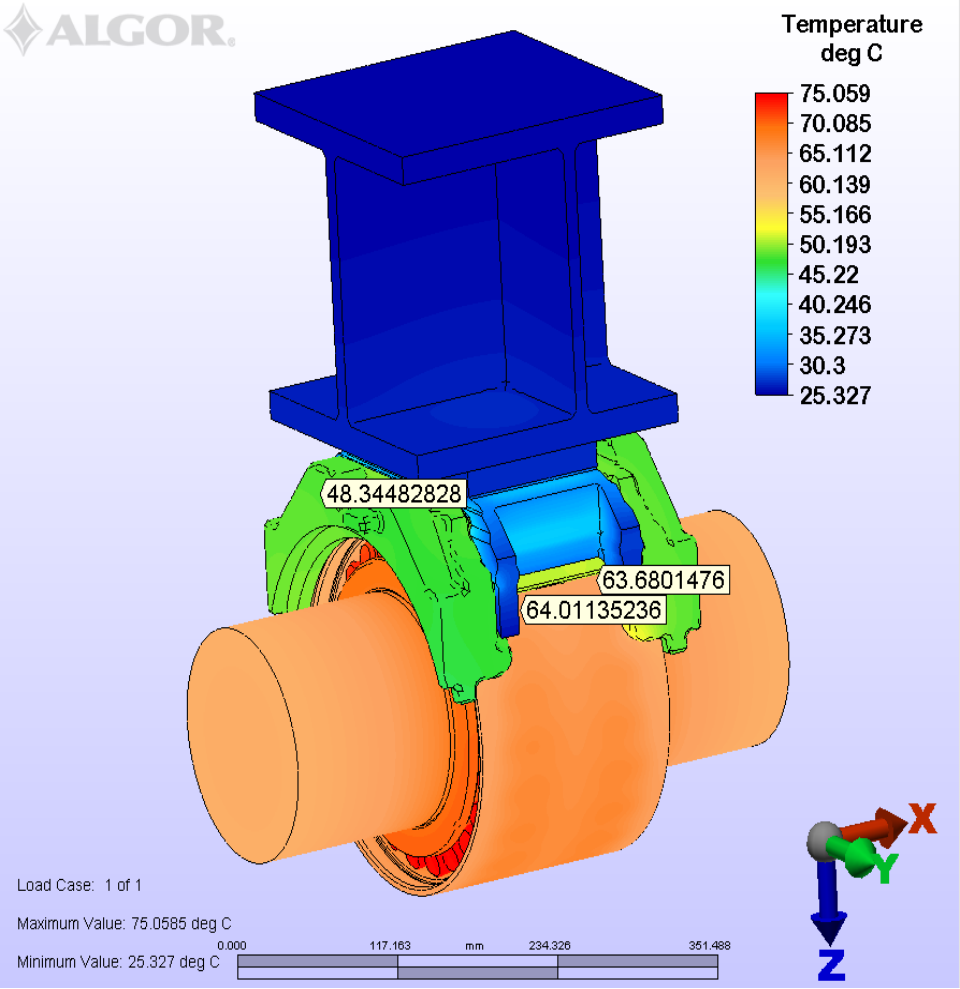

Figure 4.10. Temperature distribution of AdapterPlus™ FE model with normal operation conditions and no heat generation (ambient temperature of 25°C or 77°F).

Table 4.4. Comparison of experimental and FEA results.

Normal Operation Conditions		
Source of Results	**Thermocouple [°C / °F]**	**Bayonet [°C / °F]**
Experimental	44.2 / 111	65.4 / 150
FEA	48.4 / 119	64.1 / 147
% Difference	9.5	2

For the simulation presented in Figure 4.10, the suspension elastomer pad partially insulates the I-beam from the bearing assembly reducing its ability to act as a heat sink. Since

heat tends to transfer through the path of least resistance, most of the heat will be conducted through the axle rather than the I-beam, which justifies the axle length chosen for this FE model.

A temperature map of the AdapterPlus™ elastomer suspension pad was also obtained through FEA. Figure 4.11 and Figure 4.12 provide, respectively, the bottom and top surface temperature maps of the suspension pad during normal operation conditions. The figures demonstrate that most of the heat from the adapter is dissipated by convection along the sides of the adapter, while significantly less heat is dissipated by conduction through the central rectangular area on the bottom surface of the suspension pad. The latter becomes apparent when comparing the temperatures of the bottom and top surfaces of the elastomer suspension pad (refer to Figure 4.11 and Figure 4.12). It is evident that most of the heat is partially insulated from the I-beam and spacer plate. The temperature map of the thermoplastic elastomer suspension pad was obtained for normal operation conditions and was compared to that of previous studies [4]. The study concluded that the bottom surface of the suspension pad experiences the highest temperatures reaching about 51ºC (123.8ºF), which can be seen from Figure 4.11.

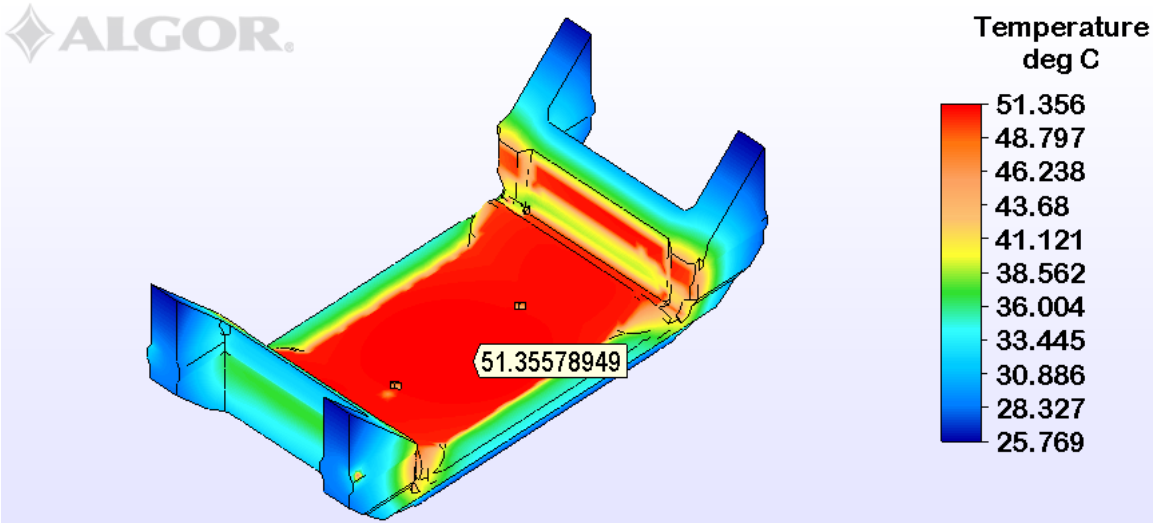

Figure 4.11. Bottom surface temperature distribution and maximum temperature of the suspension pad with normal operation conditions.

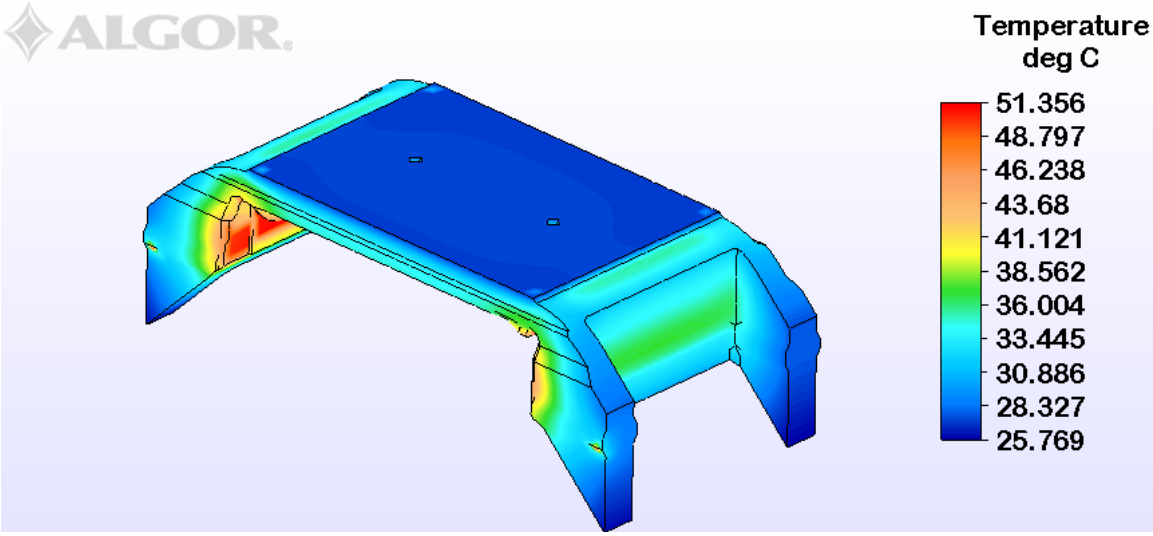

Figure 4.12. Top surface temperature distribution of the suspension pad with normal operation conditions.

4.3.3 FEA with Suspension Pad Heat Generation for Normal Operation Conditions

Figure 4.13 presents the temperature map of the AdapterPlus™ FE model when a constant heat generation due to a loading frequency of 10 Hz is applied. When compared to the simulation results presented in Figure 4.10, the results in Figure 4.13 show almost no change in the temperature distribution of the bearing assembly, adapter, or suspension pad. Table 4.5

provides the temperature difference of the locations of interest (refer to Figure 4.9) between the two different model simulations.

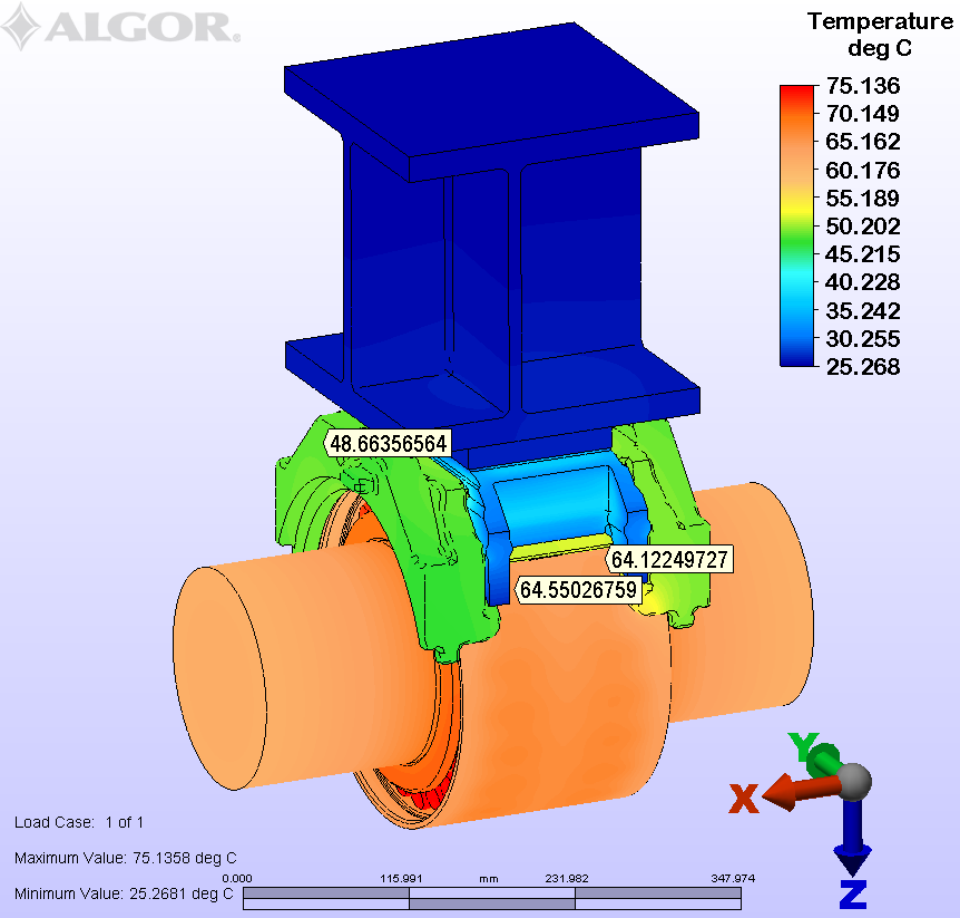

Figure 4.13. Temperature distribution of AdapterPlus™ FE model with an applied heat generation due to a frequency loading of 10 Hz and normal operation conditions (ambient temperature of 25°C or 77°F).

Table 4.5. AdapterPlus™ FE model temperature comparison (no pad heat generation versus 10 Hz pad heat generation).

Normal Operation Conditions			
Operation Condition	**Bayonet [°C / °F]**	**Thermocouple [°C / °F]**	**Pad [°C / °F]**
Heat Generation	64.4 / 147.92	48.9 / 120.02	51.6 / 124.88
No Heat Generation	64.1 / 147.38	48.4 / 119.12	51.4 / 124.52
ΔT [°C]	0.3 / 0.54	0.5 / 0.9	0.2 / 0.36

Figure 4.14 and Figure 4.15 provide, respectively, the bottom and top surface temperature maps of the suspension pad during normal operation conditions with an applied heat generation due to a loading frequency of 10 Hz. Although the maximum pad temperature is nearly the same for the two simulations (i.e. with and without pad heat generation), the temperature distribution within the pad differs markedly. Comparing the two simulations, it can be observed that the maximum temperature at the bottom surface shifts from the center of the pad (Figure 4.11) to the pad interlocks (Figure 4.14). Moreover, the temperature of the top surface of the pad is warmer for the simulation with pad heat generation (Figure 4.15) compared to the simulation with no pad heat generation (Figure 4.12).

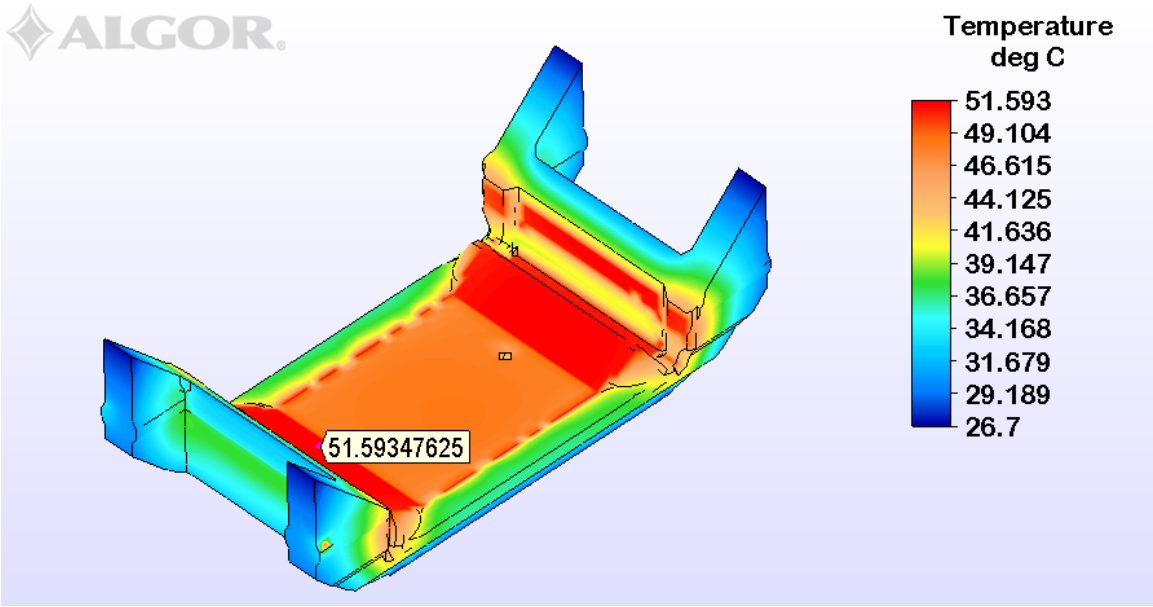

Figure 4.14. Bottom surface temperature distribution and maximum temperature of the suspension pad with normal operation conditions and an applied constant heat generation due to a frequency loading of 10 Hz.

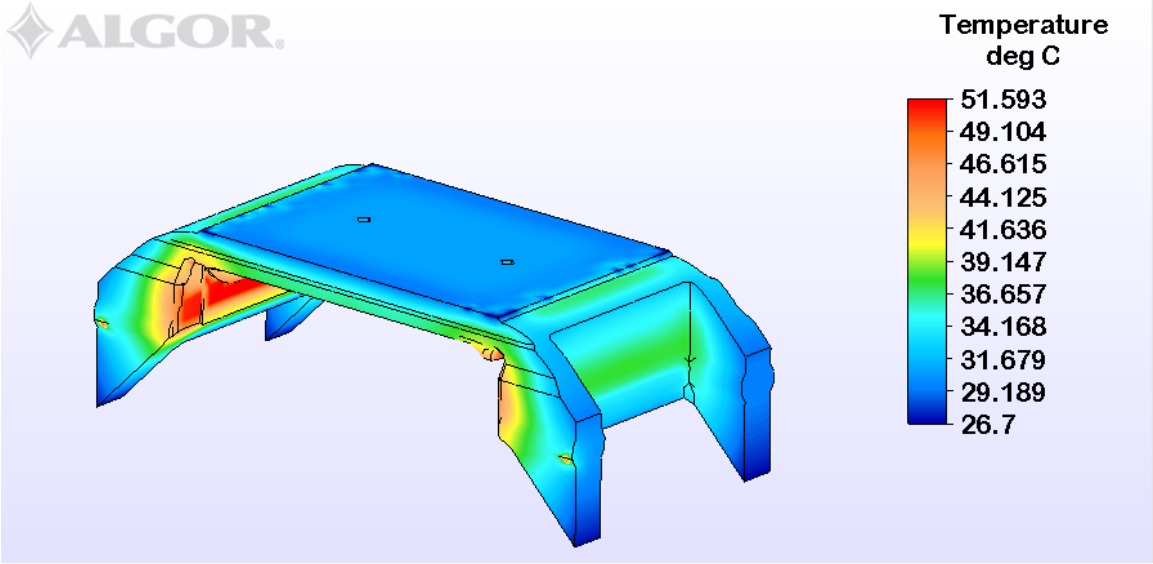

Figure 4.15. Top surface temperature distribution of the suspension pad with normal operation conditions and an applied constant heat generation due to a frequency loading of 10 Hz.

Figure 4.16 gives the temperature map of the AdapterPlus™ FE model when a constant heat generation due to a loading frequency of 50 Hz is applied. The results of this simulation compared to those in Figure 4.10 and Figure 4.13 show that the higher applied pad heat generation does not significantly affect the temperature distribution of the bearing assembly or the adapter. However, the temperature distribution of the suspension pad is affected. Figure 4.17 shows that the maximum temperature of the pad increases by 4°C (7.2°F), and the region of maximum temperature at the bottom surface of the pad shifts to the pad legs. Table 4.6 displays the temperature difference between the model with no applied heat generation in the suspension pad and the model with an applied constant heat generation due to a frequency loading of 50 Hz.

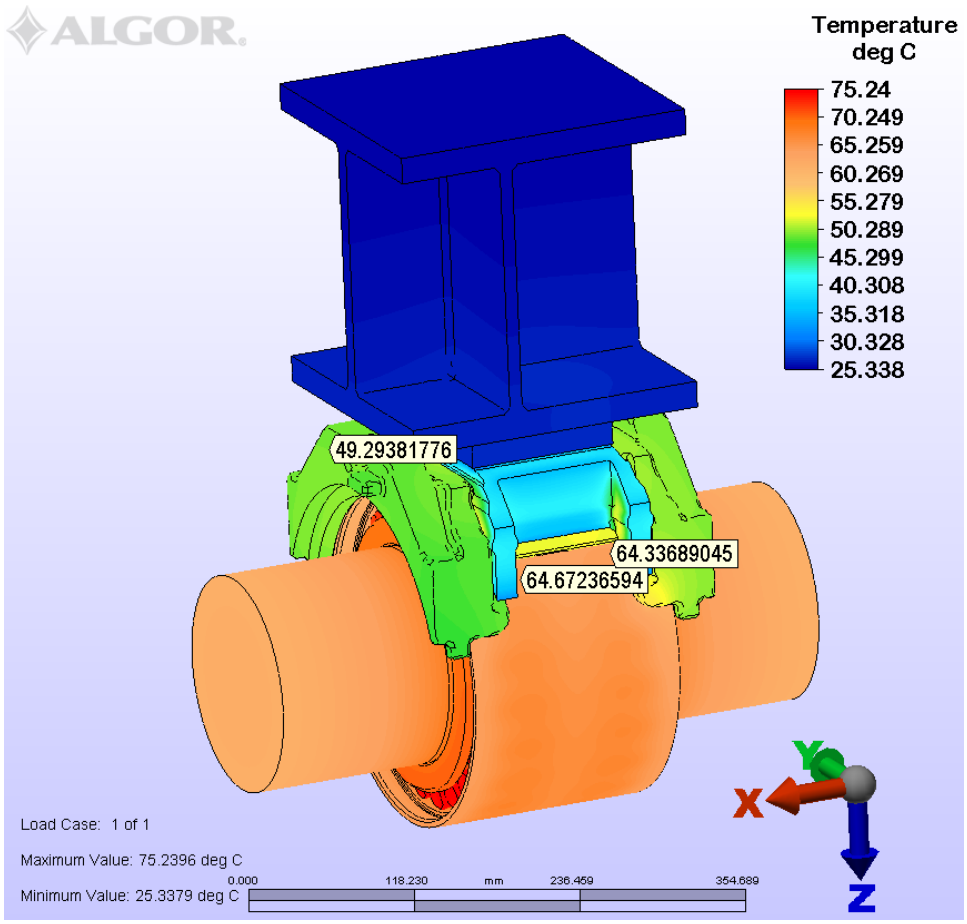

Figure 4.16. Temperature distribution of AdapterPlus™ FE model with an applied heat generation due to a frequency loading of 50 Hz and normal operation conditions (ambient temperature of 25°C or 77°F).

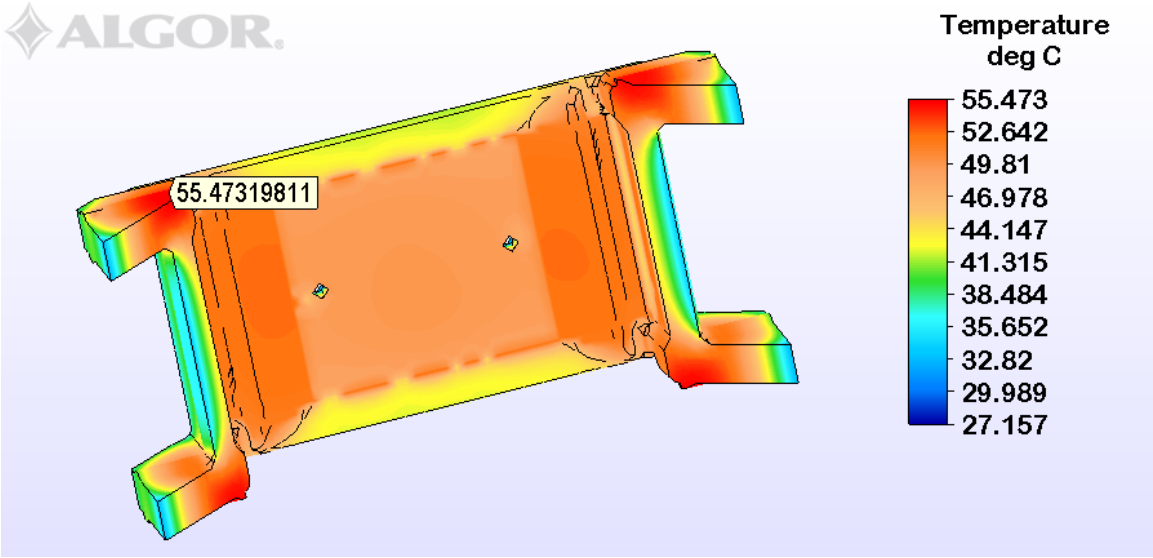

Figure 4.17. Bottom surface temperature distribution and maximum temperature of the suspension pad with normal operation conditions and an applied constant heat generation due to a frequency loading of 50 Hz.

Table 4.6. AdapterPlus™ FE model temperature comparison (no pad heat generation versus 50 Hz pad heat generation).

Normal Operation Conditions			
Operation Condition	**Bayonet [°C / °F]**	**Thermocouple [°C / °F]**	**Pad [°C / °F]**
Heat Generation	64.5 / 148.1	49.3 / 120.74	55.5 / 131.9
No Heat Generation	64.1 / 147.38	48.4 / 119.12	51.4 / 124.52
ΔT [°C]	0.4 / 0.72	0.9 / 1.62	4.1 / 7.38

4.3.4 FEA Modeling with Suspension Pad Heat Generation for Abnormal Operation Conditions

Figure 4.18 presents the temperature distribution map of the AdapterPlus™ FE model with abnormal operation conditions and no applied pad heat generation. The figure shows a significantly higher overall temperature distribution for the system, which is mainly due to the increased roller heat flux and ambient temperature. Figure 4.19 and Figure 4.20 provide the temperature distribution of the models with applied pad heat generation of 10 and 50 Hz, respectively. Interestingly, the temperature distribution results for the models with applied heat generation due to frequency loadings of 10 and 50 Hz do not exhibit a significant increase in

temperature at the locations of interest compared to the model with no applied heat generation presented in Figure 4.10, as summarized in Table 4.7.

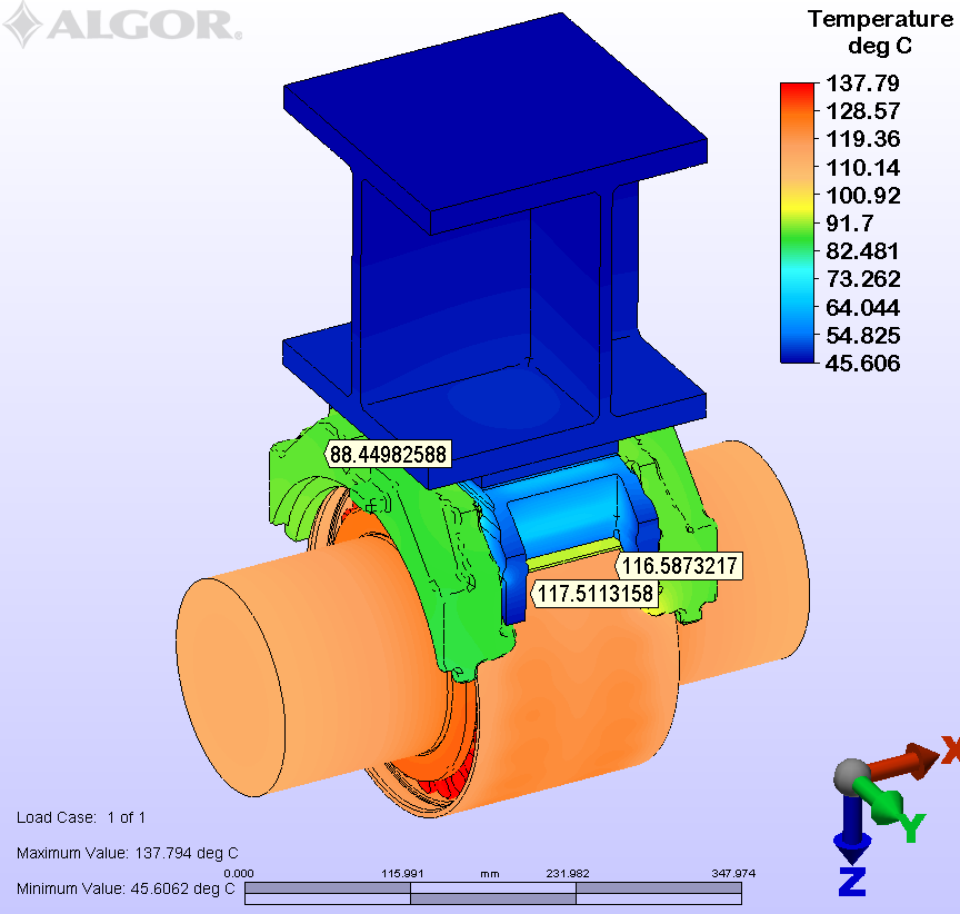

Figure 4.18. Temperature distribution of AdapterPlus™ FE model with abnormal operation conditions and no applied pad heat generation (ambient temperature of 45°C or 113°F).

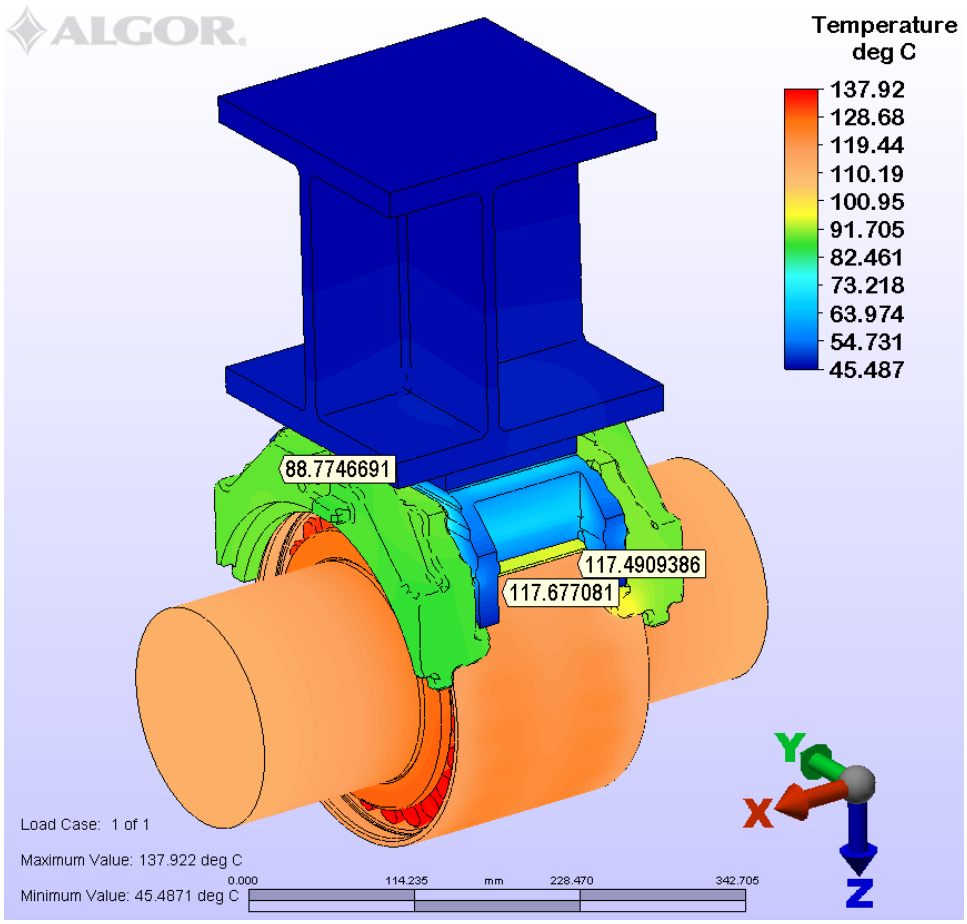

Figure 4.19. Temperature distribution of AdapterPlus™ FE model with an applied heat generation due to a frequency loading of 10 Hz and abnormal operation conditions (ambient temperature of 45°C or 113°F).

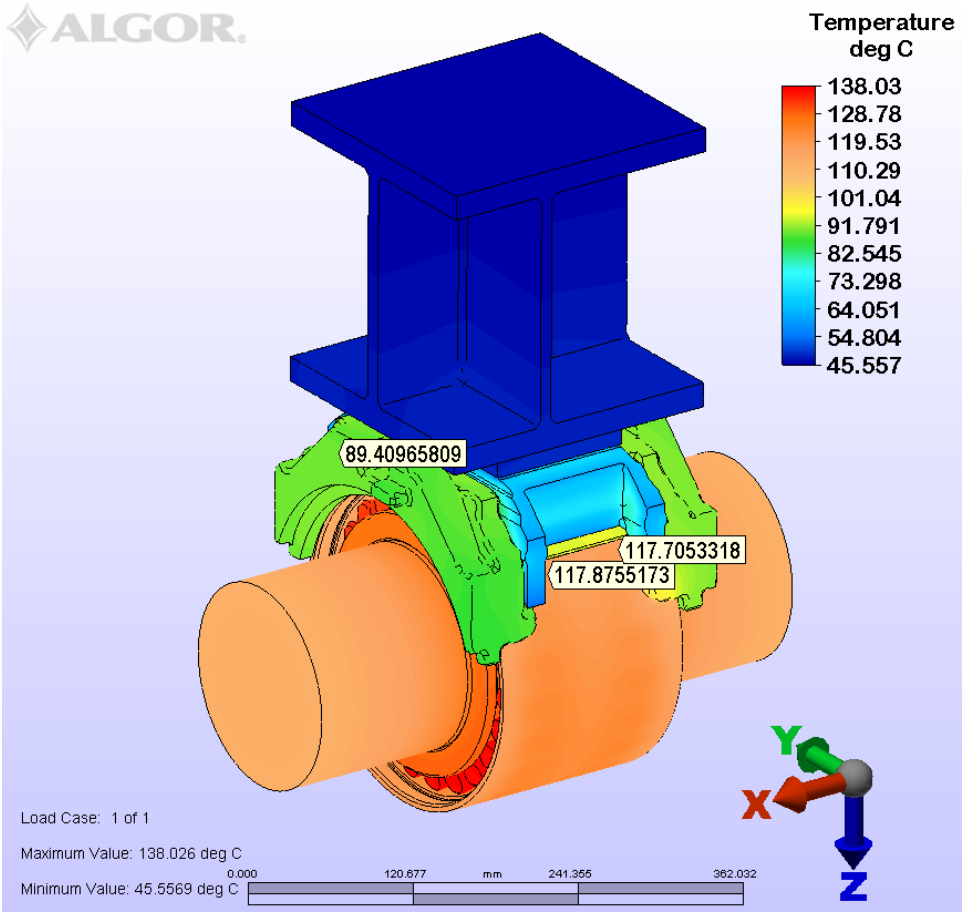

Figure 4.20. Temperature distribution of AdapterPlus™ FE model with an applied heat generation due to a frequency loading of 50 Hz and abnormal operation conditions (ambient temperature of 45°C or 113°F).

Table 4.7. AdapterPlus™ FE model temperature comparisons.

Abnormal Operation Conditions			
Applied Pad Heat Generation	**Bayonet [°C / °F]**	**Thermocouple [°C / °F]**	**Pad [°C / °F]**
None	117.1 / 242.8	88.4 / 191.1	93.9 / 201
10 Hz Loading	117.7 / 243.9	88.8 / 191.8	94.2 / 201.6
50 Hz Loading	117.8 / 244	89.4 / 192.9	95.0 / 203
Maximum ΔT [°C]	0.7 / 1.2	1.0 / 1.8	1.1 / 2

Figure 4.21, Figure 4.22, and Figure 4.23 display the abnormal operation condition temperature distribution along with the maximum surface temperature of the suspension pad for the model with no heat generation applied to the pad, the model with an applied heat generation

due to a frequency loading of 10 Hz, and the model with an applied heat generation due to a frequency loading of 50 Hz, respectively. Again, the temperature maps clearly demonstrate the shift in the location of maximum temperature within the bottom surface of the suspension pad, described earlier. Table 4.8 provides a summary of the temperatures of the locations of interest for each of the models.

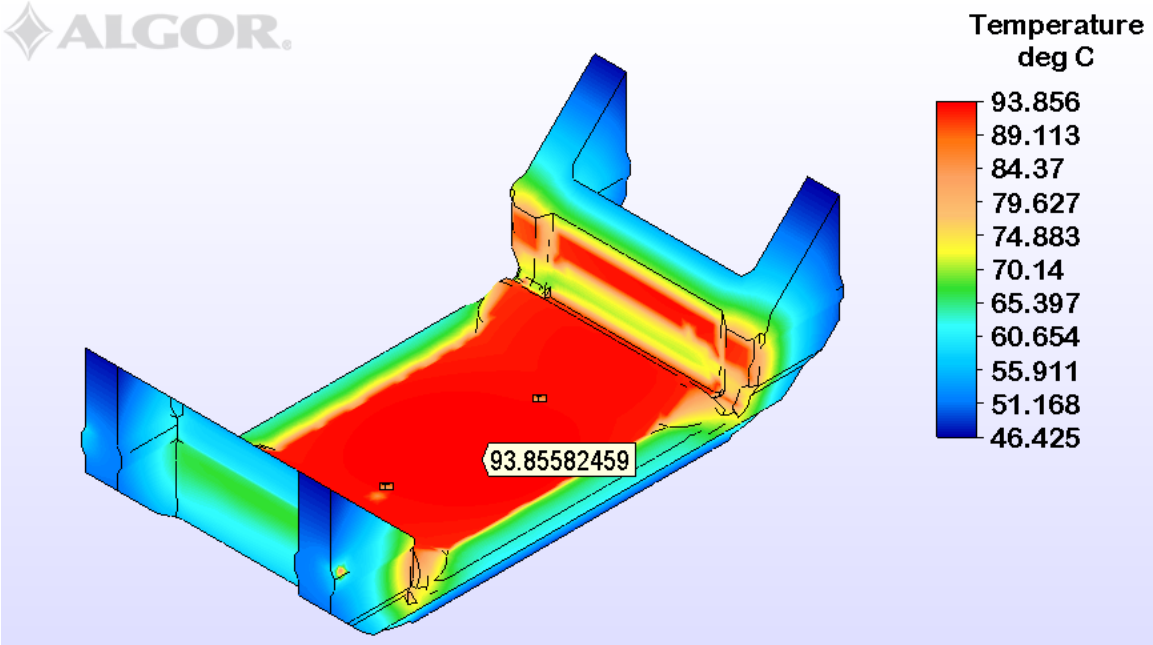

Figure 4.21. Bottom surface and maximum temperature of the suspension pad with abnormal operation conditions and no applied pad heat generation.

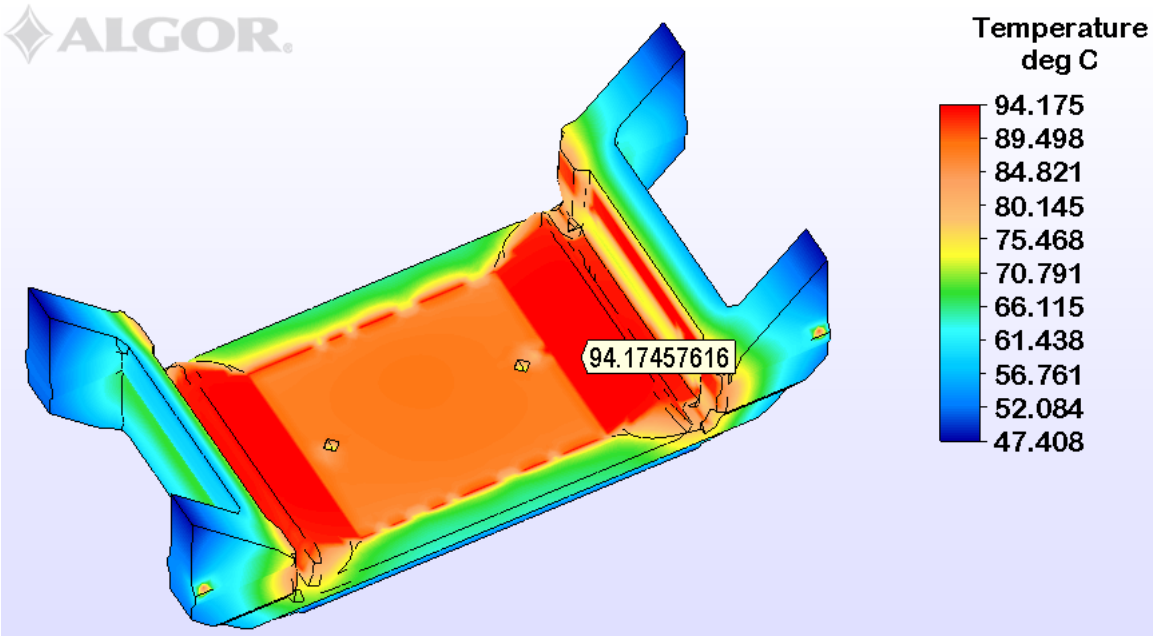

Figure 4.22. Bottom surface and maximum temperature of the suspension pad for abnormal operation conditions with applied heat generation due to a frequency loading of 10 Hz.

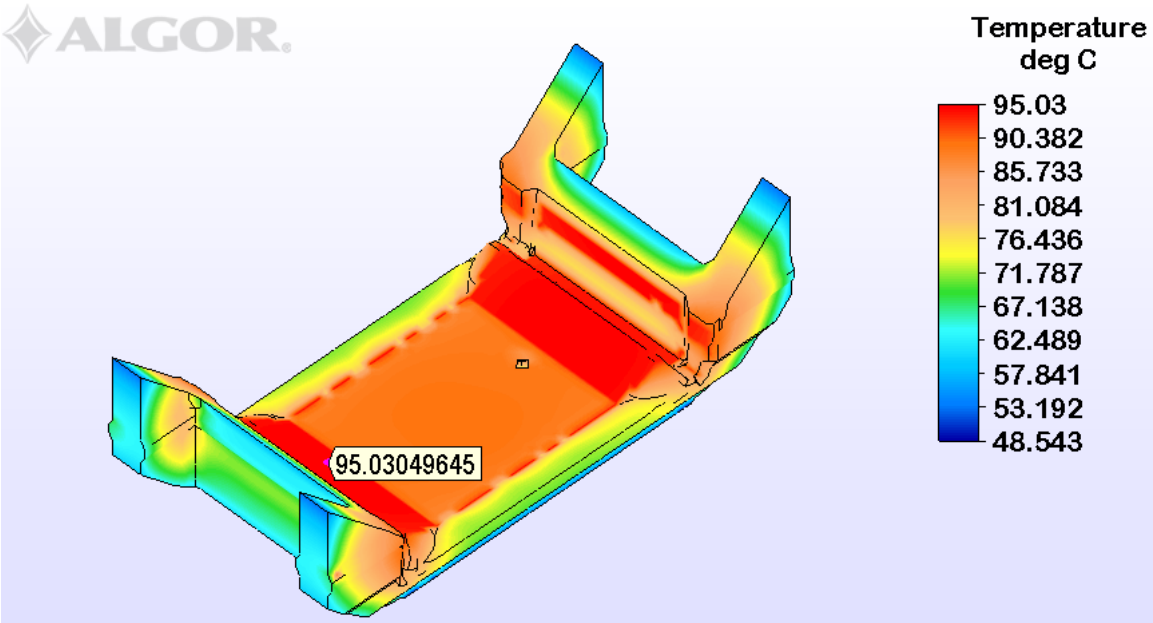

Figure 4.23. Bottom surface and maximum temperature of the suspension pad for abnormal operation conditions with applied heat generation due to a frequency loading of 50 Hz.

Table 4.8. AdapterPlus™ FE model temperature comparisons.

Abnormal Operation Conditions			
Applied Pad Heat Generation	**Bayonet [°C / °F]**	**Thermocouple [°C / °F]**	**Pad [°C / °F]**
None	117.1 / 242.8	88.4 / 191.1	93.9 / 201
10 Hz Loading	117.7 / 243.9	88.8 / 191.8	94.2 / 201.6
50 Hz Loading	117.8 / 244	89.4 / 192.9	95.0 / 203
Maximum ΔT [°C]	0.7 / 1.2	1.0 / 1.8	1.1 / 2

CHAPTER V

CONCLUSIONS

The commonly used AdapterPlus™ thermoplastic elastomer pad does generate heat under cyclic loading. The peak frequencies for heat generation are at the high end of those commonly seen in rail service and the dissipation efficiency is not particularly high. The commonly used thermoplastic elastomer pad presents an elastically dominant behavior (i.e. elastic modulus is greater than loss modulus). The loss modulus or energy dissipating behavior can be treated as independent of strain level and DMA measurement of effects of temperature and frequency are adequate for purposes of system modeling.

An experimentally validated AdapterPlus™ FE model was devised to investigate the effect of elastomer pad hysteresis heating on the railroad bearing assembly operating temperature. Different internal heating scenarios were simulated with the purpose of obtaining the bearing suspension element and bearing assembly temperature distribution maps during normal and abnormal operation conditions along with no pad heat generation and applied heat generation in the thermoplastic elastomer suspension element. The combination of temperature and frequency dependent material properties with FEA modeling permits the transient modeling and determination of the equilibrium temperature of an elastomeric steering pad. Results indicate that the combination of ambient temperature, bearing temperature, and frequency of loading can produce pad temperature increases above ambient of up to 125ºC (225ºF) if no thermal runaway is available for the pad to release the heat. The results also show that in normal and abnormal

operation conditions, the internal heat generation in the thermoplastic elastomer suspension element has limited impact on the thermal behavior of the railroad bearing assembly as long as the pad is able to dissipate heat through the side frame of the railcar. The AdapterPlus™ FE model also shows that with normal operation conditions, the temperature distribution of the suspension pad remains relatively the same when heat generation is applied. However, the constant heat generation due to a frequency loading of 50 Hz does cause the maximum temperature of the pad to increase by about 4°C (7.2ºF). Although this minor increase in temperature is not significant to the temperature distribution of the suspension pad nor does it significantly impact the thermal management or temperature distribution of the bearing assembly, the results indicate that if a significant amount of energy is generated by the suspension pad with no thermal runway, it can highly impact the structural integrity of the suspension pad.

Hysteresis heating is a phenomenon that occurs in service, and may have a significant impact on the structural integrity of the thermoplastic elastomer suspension pad, which can negatively affect the thermal management of the railroad bearing. With proper convection and normal bearing operation conditions, the heat generation will not have a significant effect. However, when a bearing becomes defective coupled with rail-track conditions that produce high frequency loading, and the ambient temperature is high, the thermoplastic elastomer suspension pad may reach temperatures higher than the softening temperature (i.e. 120ºC or 248ºF). The problem is further compounded by the reality that load and, thus, strain are not uniformly distributed on the pad. If softening occurs in the steering pad, areas under higher stress may deform significantly and shift the applied load to other areas of the steering pad, which may compromise the overall structural integrity. The latter may lead to undesired consequences and

catastrophic failure of the thermoplastic elastomer suspension element, which in turn, may hasten the catastrophic failure of the railroad bearing, leading to a costly train derailment.

Finally, this work provides a deeper understanding about the limited impact of the hysteresis heating of the railroad bearing thermoplastic elastomer suspension element on the thermal behavior of the railroad bearing assembly (under assumed conditions). This is important for proper sensor selection and placement within the bearing adapter in order to assure the efficiency of the continuous health monitoring of the railroad bearing.

REFERENCES

[1] 2.09 - Train Accidents and Rates | Federal Railroad Administration, Office of Safety Analysis. Web. safetydata.fra.dot.gov/OfficeofSafety/publicsite/query/TrainAccidentsFYCYWithRates.aspx.

[2] Tarawneh, C., et al. "Thermal Modeling of a Railroad Tapered-Roller Bearing Using Finite Element Analysis." *Journal of Thermal Science and Engineering Applications*, vol. 4, no. 3, pp. 9-19, 2012.

[3] Tarawneh, C., Cole, K., Wilson, B.M., Alnaimat, F., "Experiments and Models for the Thermal Response of Railroad Tapered-Roller Bearings," *International Journal of Heat and Mass Transfer*, Vol. 51, pp. 5794-5803, 2008.

[4] Zagouris, A., Fuentes, A. A., Tarawneh, C., Kypuros, J. A., and Arguelles, A. P., "Experimentally Validated Finite Element Analysis of Railroad Bearing Adapter Operating Temperatures," *Proceedings of the 2012 ASME IMECE Conference*, IMECE2012-88639, Houston, TX, November 9-15, 2012.

[5] Adapter Plus Steering Pad System | Amsted Rail. Web. http://www.amstedrail.com/adapter-plus-steering-pad-system

[6] Rittel, D. An Investigation of the Heat Generated during Cyclic Loading of Two Glassy Polymers. Part I: Experimental. Mechanics of Materials 32 (2000): 131-47.

[7] Rittel, D., N. Eliash, and J.l. Halary. Hysteretic Heating of Modified Poly (methylmethacrylate). Polymer 44 (2003): 2817-822.

[8] Ramkumar, A., K. Kannan, and R. Gnanamoorthy. Experimental and Theoretical Investigation of a Polymer Subjected to Cyclic Loading Conditions. International Journal of Engineering Science 48 (2010): 101-10. Print.

[9] Logan, D. L. A First Course in the Finite Element Method. Pacific Grove, CA: Brooks/Cole, 2002.

[10] Rodriguez, O. O., et al. "Hysteresis Heating of Railroad Bearing Thermoplastic Elastomer Suspension Element," *Proceedings of the 2017 ASME Joint Rail Conference,* Philadelphia, PA, April 4-7, 2017.

[11] Incropera, F.P., Dewitt, D.P., Bergman, T.L., Lavine, A.S., *Fundamentals of Heat and Mass Transfer*. Sixth Edition, 2007, Hoboken, NJ: John Wiley & Sons, Inc.

BIOGRAPHICAL SKETCH

Oscar Rodriguez was born in McAllen, Texas, USA on August 28, 1993. He attended Pharr-San Juan-Alamo High School and obtained his high school diploma in May 2011. He later received his Bachelor of Science in Mechanical Engineering with honors at the University of Texas Rio Grande Valley in December 2015. He continued his education and began his graduate work at the University Transportation Center for Railway Safety (UTCRS) at the University of Texas Rio Grande Valley and received a Master of Science in Mechanical Engineering in May 2018. Oscar demonstrated his hard work and dedication and set an example for others working in the center. He serves as a role model for his younger siblings, one of whom is pursuing an engineering degree following in his footsteps. Oscar has received three national ASME and USDOT scholarships. He was named the 2016 Student of the Year for the UTCRS, where he competed against students from University of Nebraska-Lincoln and Texas A&M University. He was named the 2017 Graduate Student of the Year for the Mechanical Engineering Department at the University of Texas Rio Grande Valley. He was lead author and presenter for three papers that were published in the 2016, 2017, and 2018 ASME Joint Rail Conference and received the best student paper award for the 2017 ASME Joint Rail Conference, which is the highest honor given at this conference. His leadership and mentorship of other students is exemplary and he has always performed his duties and approached his academics with the greatest integrity and commitment. On top of his demanding academic and research duties, he helps his family work and run their business. Oscar can be reached by e-mail at oscarosvaldo828@gmail.com.